nature communications

Article

https://doi.org/10.1038/s41467-026-71551-4

Translation in proximity to forming autophagosomes during sustained autophagy

Received: 31 March 2023

Accepted: 24 March 2026

Published online: 10 April 2026

Check for updates

Yunping Xue[1], Kaela O'Connor[1], Karsten Nalbach[2], Alexandre Savard[1], Karyn E. King[1], Ryan C. Russell[1], Christian Behrends[2] & Derrick Gibbings[1,3,4]

Autophagy is an evolutionarily conserved catabolic process. In a process requiring a cascade of over 35 autophagy-related genes (Atg), a cupped phagophore membrane expands to surround cytoplasmic material, and seals itself to form an autophagosome, which finally fuses with lysosomes. Large numbers of autophagosomes form during stress responses, while simultaneously cells drastically reduce translation to conserve energy. Here, using proximity-labeling and Fluorescence in situ Hybridization we demonstrate that multiple mRNAs encoding proteins required for autophagy preferentially localize in proximity to forming autophagosomes. Polysome fractionation and proteomics of nascent proteins in proximity to forming autophagosomes provides evidence for the local translation of these mRNAs. Translation and the ribosome-binding protein RACK1 were required for the localization of these mRNAs to forming autophagosomes. Inhibition of translation or knockdown of RACK1 caused depletion of several proteins required for autophagy and a reduction in the number of autophagosomes. Local translation may enable a rapid, energy-efficient supply of proteins for autophagy to enable cells to massively induce autophagy while conserving energy during cell stress.

Cells have evolved to utilize the minimum energy necessary in many processes. Cells and organisms are frequently confronted with nutrient limitations accentuating the importance of energy conservation. One mechanism by which cells conserve energy is by trafficking mRNA to sites where the encoded proteins are required[1,2]. A single mRNA can be translated on average 140 times, and up to 1000 times in an hour[3]. Therefore, localizing mRNA to the needed location or subcellular compartment for translation economizes energy by transporting one mRNA instead of 100s of its protein products. Local mRNA translation also provides a rapid supply of specific proteins that can enhance the speed and efficiency of processes[1,2]. RNA localization can be accomplished through several mechanisms. Localized mRNAs often contain cis-acting elements within their 3′-UTR, which are recognized by RNA-binding proteins (RBPs) for transport. For example, the 3′UTR of *β-actin* mRNA directs it to the leading edge of cells, where the cytoskeleton is abundant as cells migrate[4]. mRNAs encoding secreted or membrane proteins are recruited to the ER during translation by nascent peptides, which bind the signal recognition particle[5,6]. It was commonly understood that spatial control of mRNA translation usually involved translation being repressed during transport[7], however recent reports suggest that, like the localization of mRNAs encoding secreted proteins to the ER, mRNA localization frequently occurs while an mRNA is being translated[8,9]. Co-translational localization of mRNAs may therefore be dictated in part by partially translated proteins emerging from ribosomes or differentiated subpopulations of ribosomes[10,11] in addition to factors binding 3′UTRs.

[1]Department of Cellular and Molecular Medicine, Faculty of Medicine, University of Ottawa, Ottawa, ON, Canada. [2]Munich Cluster for Systems Neurology (SyNergy), Medical Faculty, Ludwig-Maximilians-University München, Munich, Germany. [3]Institute for Systems Biology, University of Ottawa, Ottawa, ON, Canada. [4]Eric Poulin Centre for Neuromuscular Disease, University of Ottawa, Ottawa, ON, Canada. e-mail: gibbings@uottawa.ca

When subjected to stress, cells utilize myriad pathways to reduce energy consumption to conserve resources and promote survival. Translation consumes large amounts of cellular energy and when subjected to stress cells reduce translation by over 70% by inhibiting mTORC1[12]. At the same time that cells profoundly reduce translation, inhibition of mTORC1 strongly induces autophagy, a catabolic process devoted to the degradation of intracellular components. In autophagy an entire organelle is formed de novo within minutes, and during stress 100's of autophagosomes are formed in a cell. In this process, membrane protrudes from the endoplasmic reticulum (ER) forming an omegasome[13,14]. A membrane structure called a phagophore rapidly initiates from this and expands to engulf cytoplasmic substrates. The phagophore membrane seals itself to form an autophagosome, thereby sequestering its substrates from the cytoplasm. Subsequent fusion of autophagosomes with lysosomes degrades autophagosome contents.

The intensity of autophagy is tightly regulated by the opposing effect of mTORC1 and AMPK kinases[15]. Nutrient starvation activates AMPK kinases, which inactivate mTOR and phosphorylate ULK1 to promote the activity of the ULK1/ATG13 complex thus initiating autophagy[16]. Thus, in most systems, inhibition of mTOR leads to induction of autophagy. Once activated, the ULK1 complex triggers phagophore nucleation by phosphorylating the PI3KC3 complex (e.g., VPS34, Beclin1) and activating PI3P (phosphatidylinositol 3-phosphate) production on ER-derived omegasomes[17]. Omegasomes further mature to form phagophores, in a process guided by recruitment of DFCP1 (Double FYVE-containing protein 1) and WIPI2 (WD-repeat domain phosphoinositide-interacting 2) to PI3P[18,19]. Therefore, autophagosomes are birthed on regions of ER marked by DFCP1 and WIPI2.

The formation of autophagosomes engages over 35 Autophagy-related-genes (Atg) in a cascade that results in the covalent modification of LC3 proteins with the lipid phosphatidylethanolamine (PE), to form LC3-II, which populates the forming autophagosome membrane. Autophagy receptors like p62/sequestosome1 (SQSTM1) and NBR1 (Neighbor of BRCA1) bind LC3 and substrates for autophagy, recruiting these for engulfment by forming autophagosomes[17,20]. p62/SQSTM1, NBR1 and LC3-II are also degraded by lysosomal hydrolases together with engulfed cargoes, which is consistent with the relatively short half-lives of several autophagy-related proteins[21,22]. LC3 and its lipid modification are essential, with rare exceptions, for autophagy and thus the accumulation of LC3-II and its subsequent turnover in autophagosomes correlates with the number of autophagosomes and autophagy activity[23].During autophagy, rapid, and continuous turnover of LC3, autophagy receptors, and other proteins required for autophagy risks exhausting essential autophagy related proteins without a continuously renewed supply. Together, this evidence raises the possibility that continued translation in the vicinity of forming autophagosomes may be necessary for a continuous supply of key autophagy-related proteins to sustain autophagy during prolonged stress.

Forming autophagosomes emerge from smooth ER, which is devoid of ribosomes directly attached to the ER[24], but multiple authors have remarked that the regions surrounding omegasomes and phagophores are densely populated with ribosomes using electron microscopy (EM)[25–29]. Ribosomes can also localize to forming autophagosomes to be targeted for degradation by autophagy, in a process called ribophagy[30,31]. Whether ribosomes may also be recruited in proximity to forming autophagosomes for local translation of mRNA has not been assessed to the best of our knowledge. Besides Atg9, the other core proteins required for autophagy are neither transmembrane nor secreted proteins[32], and thus the mRNA encoding them should not be recruited to the ER by the signal recognition particle. Many mRNAs which do not encode transmembrane or secreted proteins have been observed to localize to the ER for reasons that remain unclear[6,33–35].

Here, we demonstrate that mRNAs encoding many proteins required for autophagy preferentially localize in proximity to forming autophagosomes and are translated there. Localization of these mRNAs to the forming autophagosome is dependent on the ribosome-associated protein RACK1 and enables sustained autophagy in cells undergoing stress responses.

Results

mRNAs encoding several proteins required for autophagy are proximal to forming autophagosomes

Torin1, an mTOR inhibitor, induced autophagy, as confirmed by an increased LC3-II/I ratio and the accumulation of LC3-II when lysosomal degradation was inhibited with Bafilomycin A1 (BAF), a vacuolar H+ ATPase inhibitor (Supplementary Fig. 1a). Torin1 also reduced global translation as indicated by a loss of ribosome occupancy on mRNAs in polysome fractionation experiments (Supplementary Fig. 1b). To assess whether translation occurs in proximity to phagophores, or forming autophagosomes, we first validated markers of these structures. When autophagy is induced, DFCP1 and WIPI1, a marker of phagophores, co-localized (Supplementary Fig. 1c).

APEX2, an engineered ascorbate peroxidase, catalyzes the oxidation of biotin-phenol (BP) in a reaction potentiated by a 1-min pulse of H_2O_2. This generates short-lived biotin radicals that covalently ligate to nearby molecules within a 20 nm radius[36,37]. Molecules in proximity to APEX2-DFCP1 or -LC3B were biotinylated and labeled with Alexa488-streptavidin. These formed discrete foci only in cells treated with H_2O_2, and these colocalized with DFCP1 or LC3B, respectively, confirming the specificity of this proximity-based biotinylation (Fig. 1a). p62, in addition to being an autophagy receptor, also is recruited during the early steps of autophagosome formation[38,39] and a fraction of p62 puncta co-localized with biotinylation mediated by APEX2-DFCP1 (Supplementary Fig. 1d). In cells expressing APEX2-myc-DFCP1, APEX2-biotinylated signals colocalized with myc-DFCP1(Supplementary Fig. 1e). In addition, ATG14 proteins were successfully pulled down by APEX2-DFCP1-based proximity labeling and pulldown (Supplementary Fig. 1f). These results further confirmed the specificity of APEX2 proximity labeling. Cellular RNAs retrieved by proximity-labeling of APEX2-DFCP1 were detected in a manner dependent on activation of APEX2 by H_2O_2 (Supplementary Fig. 1g). In addition, the protein levels of APEX2-DFCP1 and endogenous DFCP1 in APEX2-DFCP1 expressing cells were similar with or without Torin1 ± BAF treatment (Supplementary Fig. 1h). More proteins biotinylated by APEX2-DFCP1 were observed in pulldown comparing to input samples under Torin1 conditions, which validated successful proximity labeling-based pulldown under Torin1 treatment (Supplementary Fig. 1i). mRNAs proximity-labeled by APEX2-DFCP1 and LC3B were enriched with streptavidin coated beads and quantified by RT-qPCR. Phagophores form from smooth ER which lacks ribosomes, but may be within proximity labeling distance of some rough ER. mRNA encoding transmembrane EGFR (Epidermal Growth Factor Receptor), exhibited minimal and insignificant enrichment in proximity to DFCP1 or LC3B (Fig. 1b, c). Similarly, mRNA encoding a nuclear protein, Histone H1.1 was not enriched at these sites (Fig. 1b, c). mRNAs encoding proteins participating in autophagosome formation, including ATG3, ATG12, VPS34, DFCP1 and p62 were enriched in proximity to DFCP1, even though these proteins lack transmembrane domains (Fig. 1b). Some of these mRNAs were also enriched in proximity to APEX2-LC3B (Fig. 1c). *18S* rRNA was also found enriched near DFCP1 (Fig. 1b), suggesting that mRNAs may be actively translated in proximity to the phagophore. To confirm these Atg mRNAs are specifically recruited to regions containing DFCP1 and LC3B, we used two independent cytoplasmic APEX2-fused proteins (APEX2-Perilipin2, APEX2-Cytoplasmic-V5 tag). These constructs exhibited proximity labeling localizing as expected, but this did not co-localize with the phagophore marker DFCP1 (Supplementary Fig. 2a). In contrast,

https://doi.org/10.1038/s41467-026-71551-4

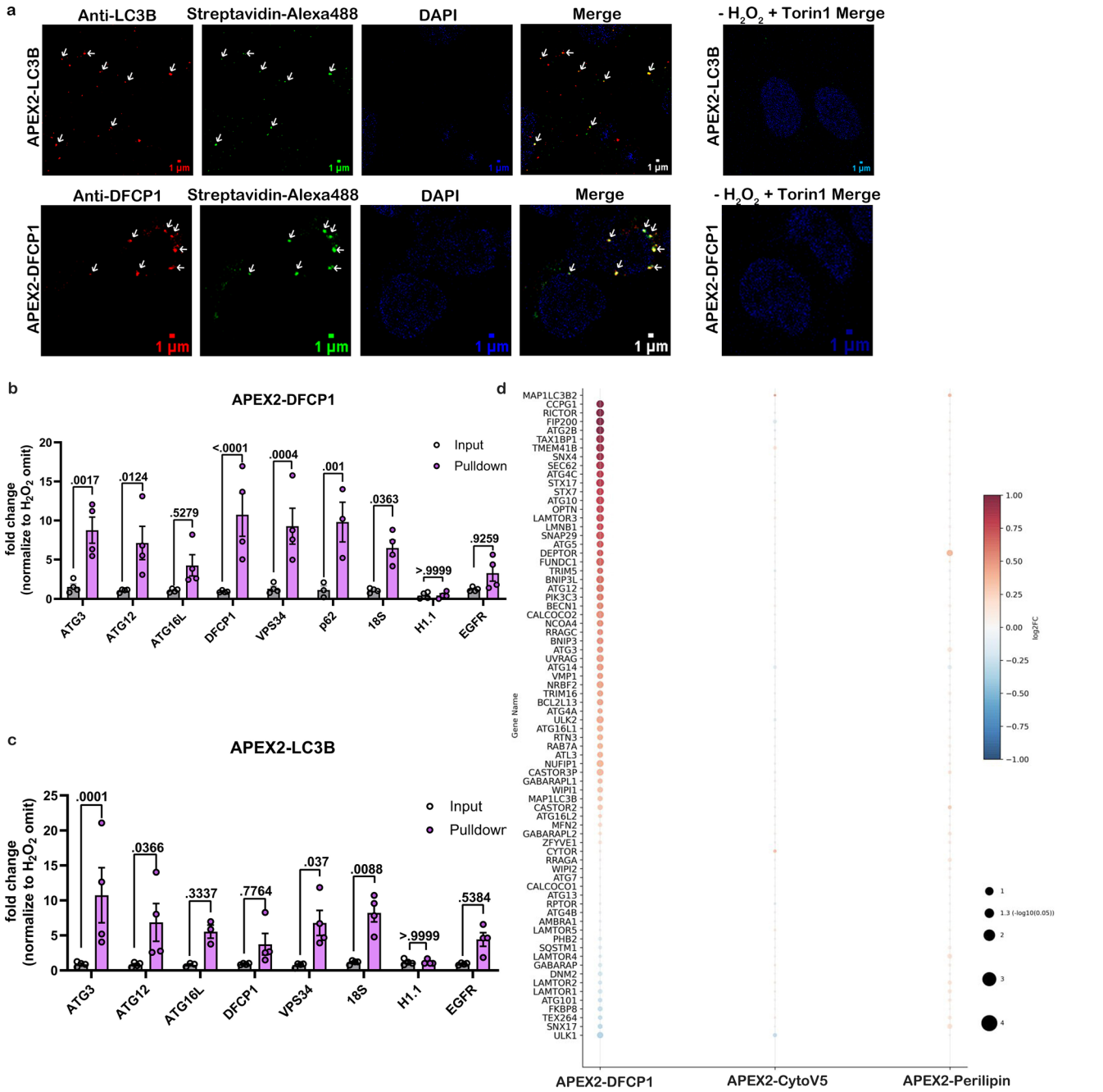

Fig. 1 | mRNAs encoding proteins required for autophagy localize in proximity to phagophores and autophagosomes. a APEX2-DFCP1 and -LC3B specifically biotinylated nearby molecules. Fluorescence microscopy of biotinylated molecules (streptavidin-Alexa488) in proximity to APEX2-DFCP1 in HEK293T cells and APEX2-LC3B in HeLa cells after treatment with Torin1 (250 nM) for 4 h. DFCP1 and LC3B signals were identified with anti-DFCP1 and anti-LC3B, respectively. **b**, **c** RT-qPCR analysis showing specific enrichment of mRNAs encoding proteins required for autophagy in proximity to DFCP1 and LC3B in cells treated with Torin1 (250 nM) for 4 h. Data are presented as mean ± standard error of the mean (SEM) from four biological replicates ($n = 4$) and were analyzed by two-way ANOVA. **d** Dot plot of candidate mRNAs encoding proteins involved in autophagy in APEX2-seq data from different subcellular locales (DFCP1, cyto-V5, and perilipin) analyzed with Limma-Voom. The enrichment level was calculated as the average ratio of (count+1) of APEX2 H_2O_2 labeling vs H_2O_2 omit. $^{****}P < 0.0001$; $^{***}P < 0.001$; $^{**}P < 0.01$; $^{*}P < 0.05$.

APEX2-DFCP1 proximity-labeling co-localized with DFCP1-mCherry (Supplementary Fig. 2a). Cytoplasmic APEX2-enriched Beta-actin mRNA by RT-qPCR as expected (Supplementary Fig. 2b). The mRNAs encoding proteins involved in autophagy which were enriched in proximity to DFCP1, were not enriched in proximity to a diffuse cytoplasmic protein (Cytoplasmic V5-tag) or Perilipin (Supplementary Fig. 2c). This demonstrates that the enrichment of these mRNAs in proximity to DFCP1 is not due to random sampling of the cytoplasm or RNA-binding sites.

To expand this principle, we performed RNAseq on mRNAs in proximity to DFCP1, CytoV5, and Perilipin. Volcano plots for DFCP1, CytoV5 and Perilipin proximity labeling demonstrate enrichment of some RNAs with each protein (Supplementary Fig. 2d). Cytoplasmic APEX2-enriched RNAs were depleted of nuclear RNAs such as *XIST* and *NEAT1*, and mRNAs that were more abundant in the nucleus in prior literature using APEX2 proximity labeling, validating the specificity of the CytoV5-APEX2 labeling (Supplementary Fig. 2d–f). mRNAs encoding an extensive list of proteins involved in autophagosome formation,

cargo recruitment and maturation were enriched in proximity to DFCP1 to a greater extent than CytoV5, or Perilipin when normalized to a negative control without H_2O_2-induction of proximity-labeling (Fig. 1d). These included mRNAs encoding ULK2, FIP200, ATG2B, ATG10, ATG12, ATG4C, VPS34 (PIK3C3), UVRAG, and TMEM41B among others. Beyond the canonical proteins involved in autophagy, mRNAs encoding additional proteins implicated in autophagy were also enriched in proximity to DFCP1. These include autophagy receptors and adapters (OPTN, CALCOCO2/NDP52, TAX1BP1, CCPG1), mitophagy mediators (FUNDC1, BNIP3L/NIX), the ER-phagy receptor SEC62, fusion-associated SNARE proteins (STX17, SNAP29, STX7), trafficking regulators (SNX4), and mTOR-associated signaling components (LAMTOR3, RICTOR).

Another set of mRNAs that encode proteins involved in autophagy processes were under-represented in proximity to DFCP1. Several of these proteins localize to sites other than the phagophore or are only involved in autophagy when selective autophagy of specific structures is triggered. For example, PHB2[40] is a protein in the inner mitochondrial membrane involved in mitophagy. TEX264 is an autophagy receptor for dsDNA breaks[41]. DNM2 is an endosomal protein[42]. SNX17 is involved in recycling components of autophagolysosomes rather than their formation[43]. LAMTOR 1, 2, 4, and 5 associate with the lysosome to anchor the RAG GTPases there[44]. Intriguingly, mRNAs encoding ULK1, ATG13, and ATG101, which form a complex involved in phagophore initiation[45], were all under-enriched in proximity to DFCP1, suggesting something unique about the localization of all mRNAs encoding this complex.

To confirm using an orthogonal method that mRNAs encoding proteins required for autophagy localize in proximity to forming autophagosomes, we used single-molecule FISH (Fluorescence In Situ Hybridization) probes for *ATG3* or *ATG12* mRNA conjugated to Quasar® 570 Dye. *ATG3* or *ATG12* mRNA frequently co-localized with or were immediately adjacent to the phagophore marker, WIPI1 (Fig. 2a–c and Supplementary Fig. 2g). *ATG3* mRNA also co-localized with DFCP1 (Supplementary Fig. 2h). In contrast, *ACTB* mRNA encoding β-actin co-localized much less frequently with WIPI1 (Fig. 2a–c and Supplementary Fig. 2g). These results reinforce the proximity-labeling data (Fig. 1b, c) demonstrating that mRNAs encoding several proteins involved in autophagy preferentially localize in proximity to phagophores.

Recruitment of mRNAs encoding autophagy proteins to DFCP1 (Fig. 2d) or LC3B (Supplementary Fig. 2i) locales required treatment with Torin1. This suggests that these mRNAs were specifically recruited to phagophores or autophagosomes, which are induced by Torin1. To test this, experiments were repeated in *FIP200*$^{-/-}$ cells. *FIP200*$^{-/-}$ cells fail to form ULK1 nucleation sites and block formation of phagophores in response to mTOR inhibition[46]. *FIP200*$^{-/-}$ cells nonetheless do not impair non-canonical autophagy pathways and their production of LC3B-II, meaning that untreated *FIP200*$^{-/-}$ cells do have LC3B-II, but this does not increase when autophagy is induced. In agreement, LC3B-II was present in *FIP200*$^{-/-}$ cells, but was not increased by Torin1 treatment (Supplementary Fig. 2j). APEX2-DFCP1 enriched mRNAs encoding autophagy-related proteins, but the enrichment of 5/6 of these was ablated in *FIP200*$^{-/-}$ cells (Fig. 2e), supporting evidence that these mRNAs localize to a site of autophagosome genesis. The enrichment of *DFCP1* mRNA in proximity to APEX2-DFCP1 was minimally affected by *FIP200*$^{-/-}$ (Fig. 2e). This is consistent with *DFCP1* mRNA localizing in proximity to APEX2-DFCP1 it encodes independent of phagophore formation. The requirement of FIP200 for localization of mRNAs to DFCP1 also shows that this is not a site involved in non-canonical autophagy processes[47], like microautophagy, LC3-associated endosomes or LC3-dependent packaging of extracellular vesicles[48,49].

mRNAs encoding proteins required for autophagy are translated near phagophores

To test for nascent protein synthesis near forming autophagosomes, APEX2-DFCP1 expressing cells were briefly pulsed with a Click-iT amino acid analog (AHA, L-azidohomoalaine) and molecules in proximity to APEX2-DFCP1 were biotinylated and pulled down. AHA was then detected on SDS-PAGE gels by coupling it to Alexa488. Nascently translated proteins were present in proximity to APEX2-DFCP1 (Fig. 3a), and this was blocked when translation was inhibited with cycloheximide (CHX, Fig. 3a). More biotinylated proteins were observed in pulldown comparing to input proteins of APEX2-DFCP1 cells treated with or without CHX, indicating successful proximity labeling and pulldown with CHX treatment (Supplementary Fig. 1i).

If proteins are translated in proximity to DFCP1, then the mRNAs should be in translation-competent ribosomes. We performed proximity labeling with APEX2-DFCP1, then polysomes were fractionated into heavy and light polysome and monosome fractions[50,51] (Supplementary Fig. 2k, l). Heavy and light polysome fractions could be ablated by EDTA, which disrupts ribosome association with mRNA[52] (Supplementary Fig. 2l). From these fractions, we pulled down biotinylated RNAs proximal to DFCP1 and performed RT-qPCR. mRNAs encoding proteins involved in autophagosome formation, like *ATG2*, *ATG3*, *ATG4*, *ATG5*, *VPS34*, *DFCP1*, *ATG12* and *p62/SQSTM* were found enriched in heavy polysome fractions in proximity to APEX2-DFCP1, while *β-actin*, mitochondrial *MTCO2*, and nuclear *H1.1* mRNAs were not (Fig. 3b). This evidence further suggests that mRNAs encoding several proteins essential for autophagy are selectively and actively translated in proximity to phagophores.

To determine which mRNAs encoding essential autophagy proteins are actively translated in proximity to phagophores, we gave a short pulse of SILAC heavy amino acids to cells, labeled and pulled-down proteins in proximity to DFCP1 and then performed mePROD mass spectrometry[12]. The significantly enriched proteins with heavy isotype labeling were mainly involved in autophagy-related pathways, indicating that the APEX2-DFCP1 successfully biotinylated proteins close to DFCP1 (Supplementary Fig. 2m). Among proteins enriched in proximity to DFCP1 versus control pulldown, a large number of ribosomal proteins from both large (with the prefix "RPL") and small ribosomal subunits (with the prefix "RPS") were identified (Supplementary Fig. 3a). VSP34, ATG5, ATG12, ATG3, p62/SQSTM, and ATG16L were identified as nascent proteins in proximity to DFCP1, with significant heavy/light amino acid (H/L) ratios (Fig. 3c). In general, the amount of nascent protein synthesis (SILAC H/L ratios) in proximity to DFCP1 correlated with the enrichment of mRNAs encoding proteins involved in autophagy (APEX2-DFCP1-seq) as shown in (Fig. 3d). Notably, ATG3, ATG5, ATG12, and PIK3C3 were significantly enriched in the APEX2-DFCP1-seq data and also exhibited strong labeling in the SILAC data, suggesting pronounced mRNA enrichment and translation of these mRNAs in proximity to DFCP1. Weaker correlation of other mRNAs with nascent peptide abundance may be attributable to differences in the translational rate or other post-transcriptional regulation among these mRNAs.

A substantial number of mRNAs without known roles in autophagy were enriched in proximity to DFCP1 in our RNAseq analysis (see Source Data file, sheet "AP2-DFCP1 RNAseq enrichment"). GO-term analysis of these mRNAs showed an enrichment for proteins involved in chromosome replication and cell cycle (Supplementary Fig. 3b). Nascent peptides were not identified for these mRNAs encoding proteins involved in cell division. This suggests a second pool of mRNAs which are not translated, may localize in proximity to phagophores.

Translation is required for sustained autophagy

If translation of proteins involved in autophagy occurs in proximity to phagophores (Fig. 3), then this translation may be required for autophagy to operate at full capacity. Previous attempts to use CHX to study the impact of translation on autophagy, were confounded by the use of serum starvation to activate autophagy[53]. CHX stops the

https://doi.org/10.1038/s41467-026-71551-4

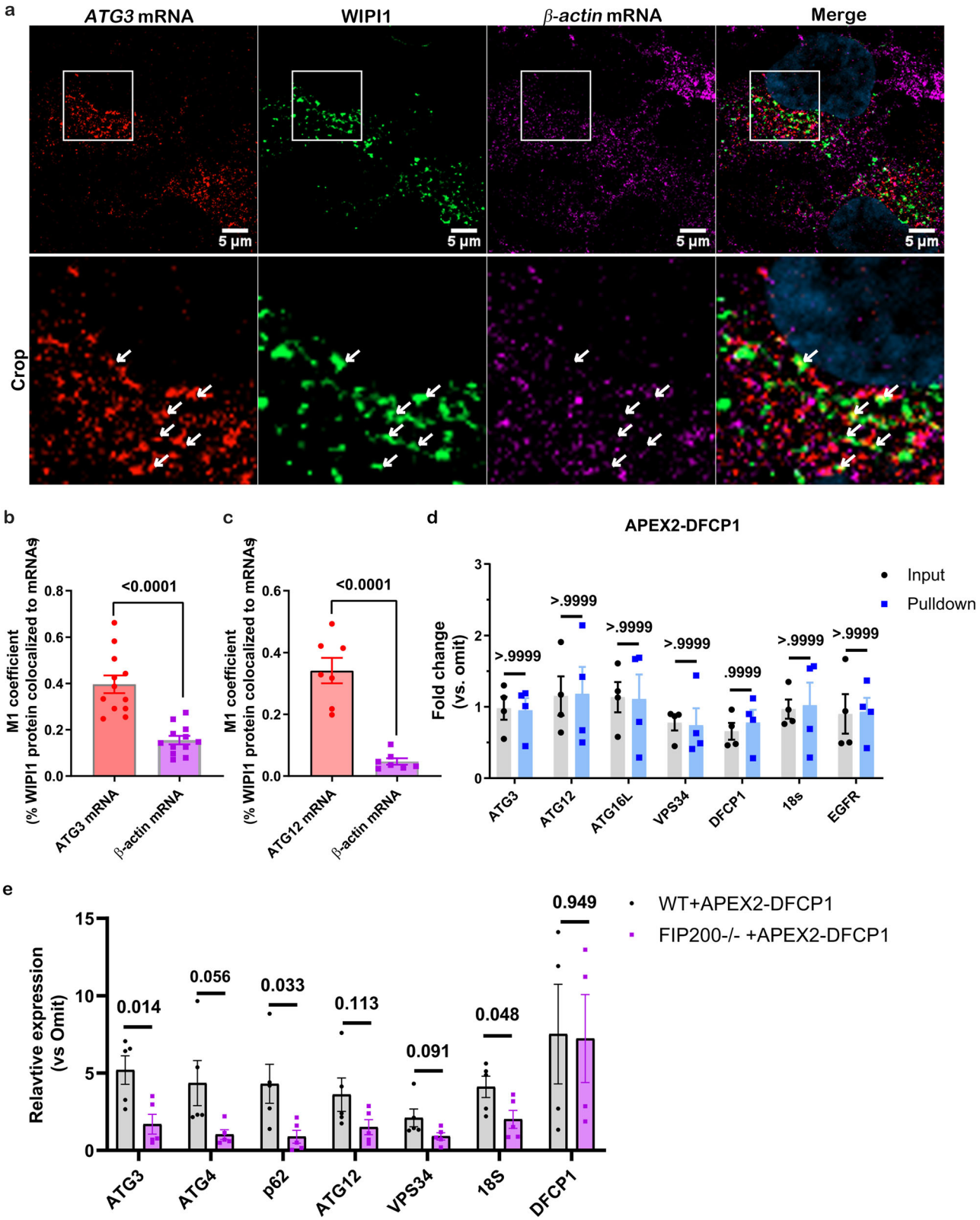

Fig. 2 | Atg mRNAs are specifically recruited to DFCP1/LC3B. *ATG3* (**a**, **b**) and *ATG12* (**c**) mRNAs colocalized more with WIPI1 proteins comparing to *β-actin* mRNAs. RNA FISH staining for *ATG3* (red), *ATG12* (red), and *β-actin* (magenta) mRNA in HeLa cells transfected with WIPI1-GFP and treated with Torin1 (250 nM) for 4 h. The white arrows indicated some of the Atg mRNAs not *β-actin* mRNAs colocalized with WIPI1. Manders' colocalization coefficient was used to quantify the percentage of mRNAs colocalized to WIPI1 proteins. Data are mean ± SEM and unpaired t-test was used for analysis (Two-sided). Data represent $n = 12$ images (**b**) and $n = 7$ images (**c**) obtained from three independent experiments (>40 cells in total were quantified). **d** RT-qPCR analysis showing no enrichment of Atg mRNAs in proximity to DFCP1 in cells without Torin1 treatment. Data are mean ± SEM and analyzed with two-way ANOVA ($n = 4$ biological replicates). **e** RT-qPCR analysis of Atg mRNAs enrichment in proximity to APEX2-DFCP1 in WT or FIP200$^{-/-}$ cells transfected with APEX2-DFCP1. Data are mean ± SEM and multiple-t test (Two-sided) was performed using $n = 5$ biological replicates.

https://doi.org/10.1038/s41467-026-71551-4

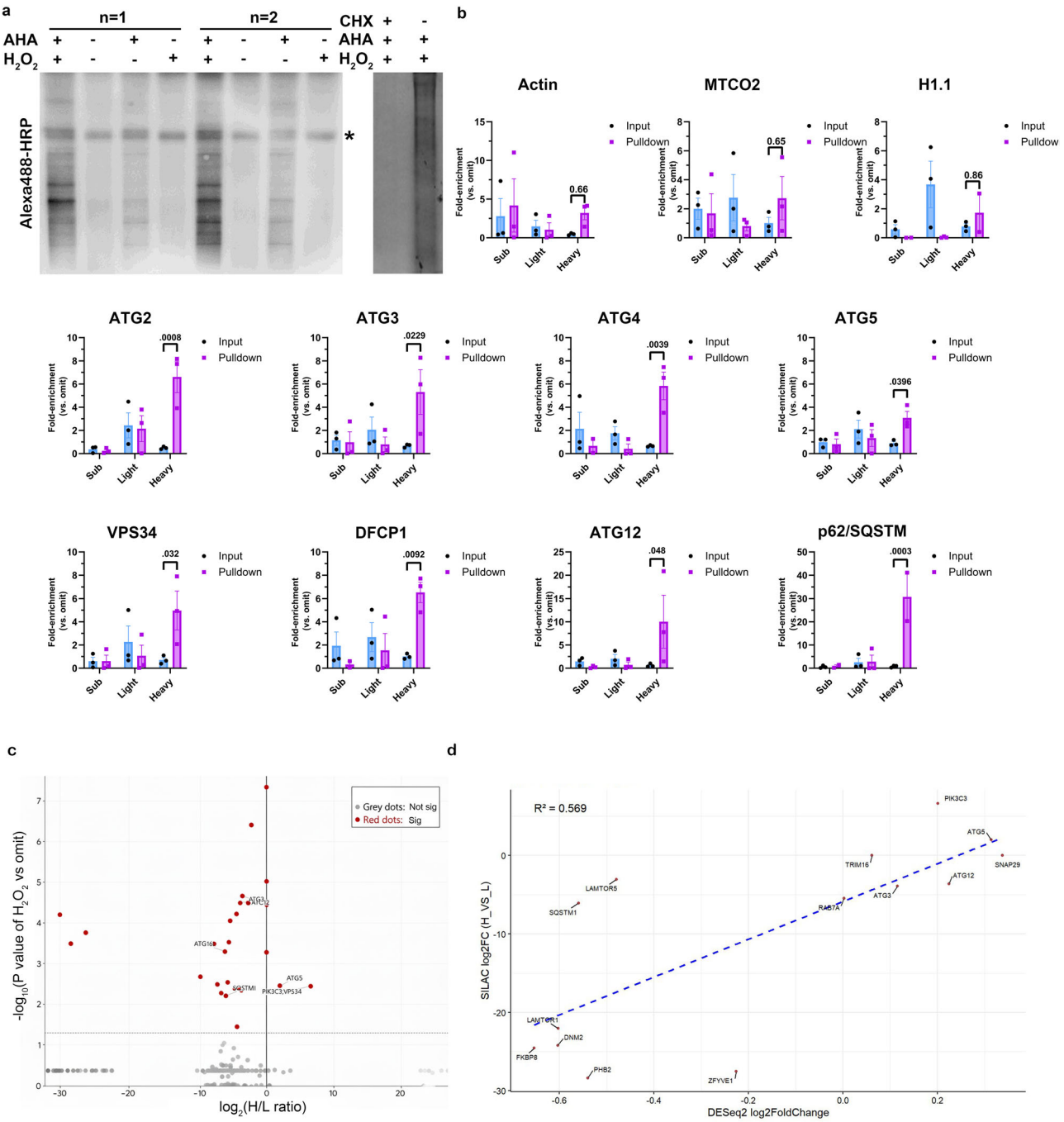

Fig. 3 | Autophagy-related mRNAs are translated at phagophores. a Detection of AHA-labeled nascent proteins clicked to Alexa488 and detected with western blot using anti-Alexa488 antibody and HRP-conjugated secondary antibody. APEX2-DFCP1 expressing cells treated with/ without CHX (100 μg/mL) were pulsed with/ without AHA and proteins in proximity to APEX2-DFCP1 were biotinylated and pulled down. *Non-specific band. **b** RT-qPCR analysis showing specific enrichment of Atg mRNAs in polysome fractions in input total samples as well as in proximity to DFCP1 (S = sub-polysome, L = light polysome, H = heavy polysome). APEX2-DFCP1 expressing cells treated with Torin1 (250 nM, 4 h) were labeled with BP ± H_2O_2. The cell lysates went through heavy polysome fractionation, pulldown with streptavidin beads and RT-qPCR to quantify polysome-associated mRNAs in proximity to DFCP1. Data are presented as mean ± SEM from three biological replicates ($n = 3$), and statistical significance was assessed using two-way ANOVA. **c** APEX2-DFCP1 cells underwent a short pulse of SILAC heavy amino acids for 30 min, proximity-labeling based pulldown, and subsequent mePROD mass spectrometry to identify nascent proteins in proximity to DFCP1. A volcano plot displaying log2 (Heavy /Light ratio) of pulldown proteins from H_2O_2 group and the p value of H_2O_2 versus H_2O_2 omit of heavy-isotype labeled samples, analyzed with independent t-tests (two-sided). Orange dots represent heavy isotype-labeled proteins that are significantly enriched in proximity to DFCP1. **d** Correlation between RNA enrichment (APEX2-DFCP1-seq) and nascent protein synthesis (SILAC H/L ratios). ****$P < 0.0001$; ***$P < 0.001$; **$P < 0.01$; *$P < 0.05$.

incorporation of amino acids into proteins, which also increases the free amino acid pool, thereby reactivating mTOR and reducing autophagy[53]. To avoid this confounding effect, mTOR inhibitors (INK128, Torin1) were used to ensure complete inhibition of mTOR during CHX treatment which was confirmed by the sustained dephosphorylation of eIF4EBP (Supplementary Fig. 3c, d).

To identify proteins involved in autophagy that continue to be translated during sustained autophagy, HeLa cells were treated with

https://doi.org/10.1038/s41467-026-71551-4

Table 1 | Reagents, equipment, and cell lines

Antibody	Vender	Cat#
LC3A	Cell Signaling Technology	4599
LC3B	Sigma-Aldrich	L7543
ATG2A	MBL	PD041
ATG3	Cell Signaling Technology	3415
ATG5	Cell Signaling Technology	8540
ATG7	Cell Signaling Technology	8558
ATG12	Cell Signaling Technology	4180
ATG16L1 (D6D5)	Cell Signaling Technology	8089
ACTB	Sigma-Aldrich	A5441
4E-BP1 (53H11)	Cell Signaling Technology	9644S
PHOSPHO-4E-BP1 (s65)	Cell Signaling Technology	9456
RACK1 (B-3)	Santa cruz	sc-17754
p62 Antibody	Sigma-Aldrich	P0067
Streptavidin-AF488	Thermo Fisher Scientific	S32354
ZFYVE1 /DFCP1	novusbio	NBP1-84267-25ul
IHC-plus™ Polyclonal Rabbit anti-Human ZFYVE1 / DFCP1 Antibody	lsbio	LS-B15646-50
Mouse IgG1 K Isotype Control Purified	eBioscience	14-4714-82
Rabbit IgG isotype control antibody	genetex	GTX35035
GAPDH	Santa cruz	sc-32233
NBR1	Abnova	H00004077-M01
NDP52	Cell Signaling Technology	9036S
OPTN/ Optineurin (C-Term) Polyclonal Antibody	Caymanchem	100000
RPS3A Antibody	Bethyl Laboratories	A305-001A-T
RPL10A Antibody	Bethyl Laboratories	A305-062A-T
Vinculin Antibody	Abcam	Ab129002
Oligonucleotides		
RACK1 Silencer Select siRNA s20340	ThermoFisher	4392420
Silencer Select Negative Control siRNA 2	ThermoFisher	4390824
RACK1 3'UTR siRNA ID 556309	ThermoFisher	4399665
Recombinant DNA	**Vender**	**Cat#**
pEGFP-N1-RACK1	Addgene	41088
mCherry-DFCP1	Addgene	86746
GFP-DFCP1	Addgene	38269
WIPI2-Halo WT	Addgene	175025
APEX2-DFCP1	Gift from Dr. Christian Behrends' lab	
APEX2-NPM1	Gift from Dr. Christian Behrends' lab	
APEX2-LC3B	Gift from Dr. Christian Behrends' lab	
APEX2-LC3B^{G120A}	Gift from Dr. Christian Behrends' lab	
WIPI1-GFP	Addgene	38272
APEX2- perilipin2	Addgene	170573

Table 1 (continued) | Reagents, equipment, and cell lines

Antibody	Vender	Cat#
APEX2-Cyto-V5	Addgene	170572
Other	**Vender**	**Cat#**
Dynabeads™ MyOne™ Streptavidin C1	Invitrogen	65001
Click-IT™ AHA (L-Azidohomoalanine)	Invitrogen	C10102
Alexa Fluor™ 488 Alkyne	Invitrogen	A10267
Click-iT® Cell Reaction Buffer Kit	Thermo Fisher Scientific	C10269
Click-iT Protein Reaction Buffer Kit	Thermo Fisher Scientific	C10276
Antifade Mounting Medium with DAPI	VECTASHIELD	H-1200-10
Mounting medium (W/o DAPI)	VECTASHIELD	H-1000
RPMI, no methionine	Gibco	A1451701
µ-slide 8 well chambered coverslip	Ibidi	80826
6-FAM-dC-puromycin	Jena Bioscience	NU-925-6FM-S
6-FAM	Invitrogen	C1360
Opti-MEM/ Reduced Serum Medium	Giboco	31985070
Lipofectamine™ RNAiMAX Transfection Reagent	Invitrogen	13778075
M-MuLV Reverse Transcriptase	NEB - New England Biolabs	M0253L
GoTaq® qPCR Master Mix	Promega	A6002
Enhanced PEI (polyethylenimine)	Biobar	R-R02
PVDF transfer membrane	Thermo Scientific	88518
Immun-Blot Low fluorescence PVDF membrane	Biorad	1620261
HaloTag® Ligands (Coumarin)	Promega	G8582
Dynabeads Protein G	Thermo Fisher	10004D
Human ATG3 mRNA probe with Quasar® 570 Dye	Biosearch technologies	SMF-1063-5
Human ATG12 mRNA probe with Quasar® 570 Dye	Biosearch technologies	SMF-1063-5
Stellaris® FISH Probes, Human ACTB with Quasar® 670 Dye	Biosearch technologies	VSMF-2003-5
dNTP Mix 10 mM	bio basic	DD0056
Salmon sperm DNA	Thermo Fisher	15632011
Baker's yeast RNA	Sigma Aldrich	R6750-100MG
Chemiluminescent Nucleic Acid Detection Module Kit	Thermo Fisher	89880
Mass-spec grade trypsin	Worthington Biochemical	LS02122
Sep-Pak tc18 1cc cartridges	Waters	WAT054960
Chemical reagent	**Vender**	**Cat#**
2-Mercaptoethanol	Bio-Rad	1610710
4× Laemmli sample buffer	Bio-Rad	161–0747
Sucrose	Fisher Scientific	BP220-1
Biotin-tyramide	Sigma Aldrich	SML2135
Doxycycline hyclate	Sigma Aldrich	D9891
Torin1	Tocris Bioscience	4247
INK128 (MLN-0128)	ChemieTek	CT-INK128
BafilomycinA1	Millipore sigma	196000-1SET
Trolox	Cayman chemicals	10011659
Sodium ascorbate	Sigma Aldrich	A7631-100G
Sodium azide	Fisher Scientific	AAJ2161022
TRIzol	Invitrogen	15596018

Table 1 (continued) | Reagents, equipment, and cell lines

Antibody	Vender	Cat#
Cycloheximide/CHX	Sigma Aldrich	C7698
H_2O_2	Fisher Scientific	H325100
Hygromycin B	Thermo Fisher	10687010
formamide	Fisher Scientific	BP227-500
Harringtonine	Cayman chemicals	15361
Stellaris® RNA FISH Hybridization Buffer	Biosearch technologies	SMF-HB1-10
HaloTag® Ligands (Coumarin)	Promega	G8585
Duolink In Situ Wash Buffers, Fluorescence	Sigma Aldrich	DUO82049
Duolink® In Situ PLA Probe Anti-Rabbit PLUS	Sigma Aldrich	DUO82002
Duolink® In Situ PLA® Probe Anti-Mouse MINUS	Sigma Aldrich	DUO82004
Duolink Antibody Diluent (1×)	Sigma Aldrich	DUO82008
Duolink® In Situ Mounting Medium with DAPI	Sigma Aldrich	DUO82040
Duolink Blocking Solution (1×)	Sigma Aldrich	DUO82007
Duolink® In Situ Detection Reagents Orange	Sigma Aldrich	DUO92007
Cell lines	**Vender**	**Cat#**
HeLa WT	ATCC	CCL2
HEK293T	ATCC	CRL-3216
HEK293T expressing LC3B-mCherry-GFP	Dr. Ryan Russel's lab	
APEX2-DFCP1 expressing HeLa cells	Dr. Christian Behrends' lab	
APEX2-LC3B expressing HeLa cells	Dr. Christian Behrends' lab	
Equipment	**Vender**	**Cat#**
Density gradient fractionation system	Brandel	SYN-202
DynaMag™–2 Magnet	Invitrogen	12321D
Quorum spinning disk confocal microscopy	Leica (provided by UOttawa CBIA core)	
Zeiss LSM800 AxioObserver Z1	Zeiss (provided by UOttawa CBIA core)	

Torin1 and BAF to negate the influence of protein turnover caused by lysosomal degradation. The cellular protein levels of ATG3, ATG5, ATG12, and ATG7 significantly decreased when translation was blocked with CHX (Fig. 4a, b). ATG2 protein levels were also decreased by CHX but with the P value of 0.056 (Fig. 4a, b). Intriguingly, the mRNA encoding ATG16L1 was minimally, or not enriched in proximity to DFCP1 (Fig. 1b), and the levels of ATG16L1 were not significantly altered by CHX (Fig. 4a, b). Notably, the levels of several autophagy receptors including p62, NBR1, OPTN (Optineurin), LC3A-II (autophagosome marker) and NDP52 (CALCOCO2) were also depleted when translation was inhibited (Fig. 4c, d). These data suggest that translation of several proteins involved in autophagy is required to maintain their levels and sustain autophagy.

To further evaluate the requirement of translation for sustained autophagy, HEK293T cells expressing a GFP-mCherry-LC3B autophagy reporter were treated with mTOR inhibitor, with or without CHX. Quenching of GFP, but not mCherry by the low pH of the lysosome enables quantification of autophagosomes and autophagolysosomes respectively[54]. Inhibition of translation reduced the numbers of both autophagosomes and autophagolysosomes (Fig. 4e–g) and this was not caused by the fluorescence intensity change of GFP and mCherry (Supplementary Fig. 3e, f).

RACK1 is required for localization of autophagy-related mRNAs to forming autophagosomes

A specific factor may be involved in recruiting mRNAs to forming autophagosomes for in situ translation. Recruitment of mRNAs encoding autophagy proteins into the vicinity of DFCP1 (Fig. 5a) and LC3B (Supplementary Fig. 3g) was abrogated when translating ribosomes were displaced from mRNAs with puromycin. Recruitment of *28S* rRNA to DFCP1 was also significantly inhibited by puromycin (Fig. 5a). *EGFR* mRNA was enriched in DFCP1 proximity labeling samples, but to a lesser extent than mRNAs encoding autophagy proteins. This enrichment was likely due to *EGFR* presence at ER (Fig. 5a). Interestingly, recruitment of several of these mRNA to DFCP1 was also abolished by Homoharringtonine (Supplementary Fig. 3h), which arrests ribosomes at the start codon and disrupts polysomes[55,56]. This indicates that autophagy-related mRNAs require ongoing translation, and potentially a ribosome-associated factor for the recruitment to or the retention at DFCP1 locales. RACK1 (Receptor for Activated C-Kinase 1, GNB2L1), which can bind the 40S small ribosomal subunit near the mRNA exit tunnel[57], was previously shown to bind to a complex of VPS15, ATG14L, and Beclin1, placing it at the site of phagophore formation[58]. RACK1 is also known to control the translation of mRNAs encoding proteins involved in autophagy[59].

In cells treated with Torin1, RACK1 immunoprecipitated mRNAs including *ATG3*, *ATG12*, *VPS34*, *p62*, and *DFCP1*, while *GAPDH*, and *β-actin* mRNAs were not significantly associated with RACK1 (Fig. 5b). By selectively associating with complexes containing these mRNAs, RACK1 is a prime candidate for recruiting these mRNAs to phagophores. In agreement, fluorescence microscopy for RACK1-GFP transfected cells demonstrated that it colocalizes with or is immediately adjacent to many puncta of DFCP1 (Fig. 5c) and co-localizes with both *ATG12* mRNA and the phagophore marker WIPI2 (Supplementary Fig. 3i). In proximity ligation assays (PLA), RACK1 proteins were also found in the vicinity of DFCP1 proteins but not Histone H3 proteins (Supplementary Fig. 3j). In addition, DFCP1 protein, ribosomal proteins (RPL7, RPL18, RPS9) and ER protein (ATP2A2/SERCA2), were immunoprecipitated by RACK1 after Torin1 treatment (Supplementary Fig. 3k). This confirms that RACK1 associates with phagophores and mRNAs encoding autophagy proteins.

Depletion of RACK1 with siRNA was validated by Western blot and RT-qPCR (Supplementary Fig. 4a, b) and did not affect cellular levels of autophagy-related mRNAs (Supplementary Fig. 4c). More proteins biotinylated by APEX2-DFCP1 were observed in pulldown comparing to input samples with or without RACK1 siRNAs transfection, indicating successful proximity labeling and pulldown under RACK1 knockdown (Supplementary Fig. 1i). RACK1 knockdown abrogated the recruitment of mRNAs essential for autophagy, including *ATG3*, *ATG12*, *VPS34*, *DFCP1* and *p62* into the vicinity of DFCP1 as detected using proximity labeling pulldowns with APEX2-DFCP1 (Fig. 5d). Similarly, *ATG3* or *ATG12* mRNA co-localized less with the phagophore marker WIPI1 by FISH when RACK1 levels were reduced (Fig. 5e, Supplementary Fig. 4d). Therefore, RACK1 is necessary for recruitment of mRNA encoding proteins involved in autophagy to phagophores. Together, these multiple lines of evidence support a model in which mRNAs encoding proteins essential for autophagy like ATG3 are recruited to forming autophagosomes in a process dependent on active translation and RACK1[60–62].

RACK1 regulates translation of autophagy-related mRNAs in proximity to phagophores

RACK1 associates with ribosomes and selectively regulates the translation of subpopulations of mRNAs[59,63,64]. Since RACK1 co-localizes with forming autophagosomes and recruits mRNAs to this site, we hypothesized that RACK1 controls translation of these mRNAs in proximity to forming autophagosomes. Knockdown of RACK1 detectably diminished levels of translation in cells, as detected by polysome

https://doi.org/10.1038/s41467-026-71551-4

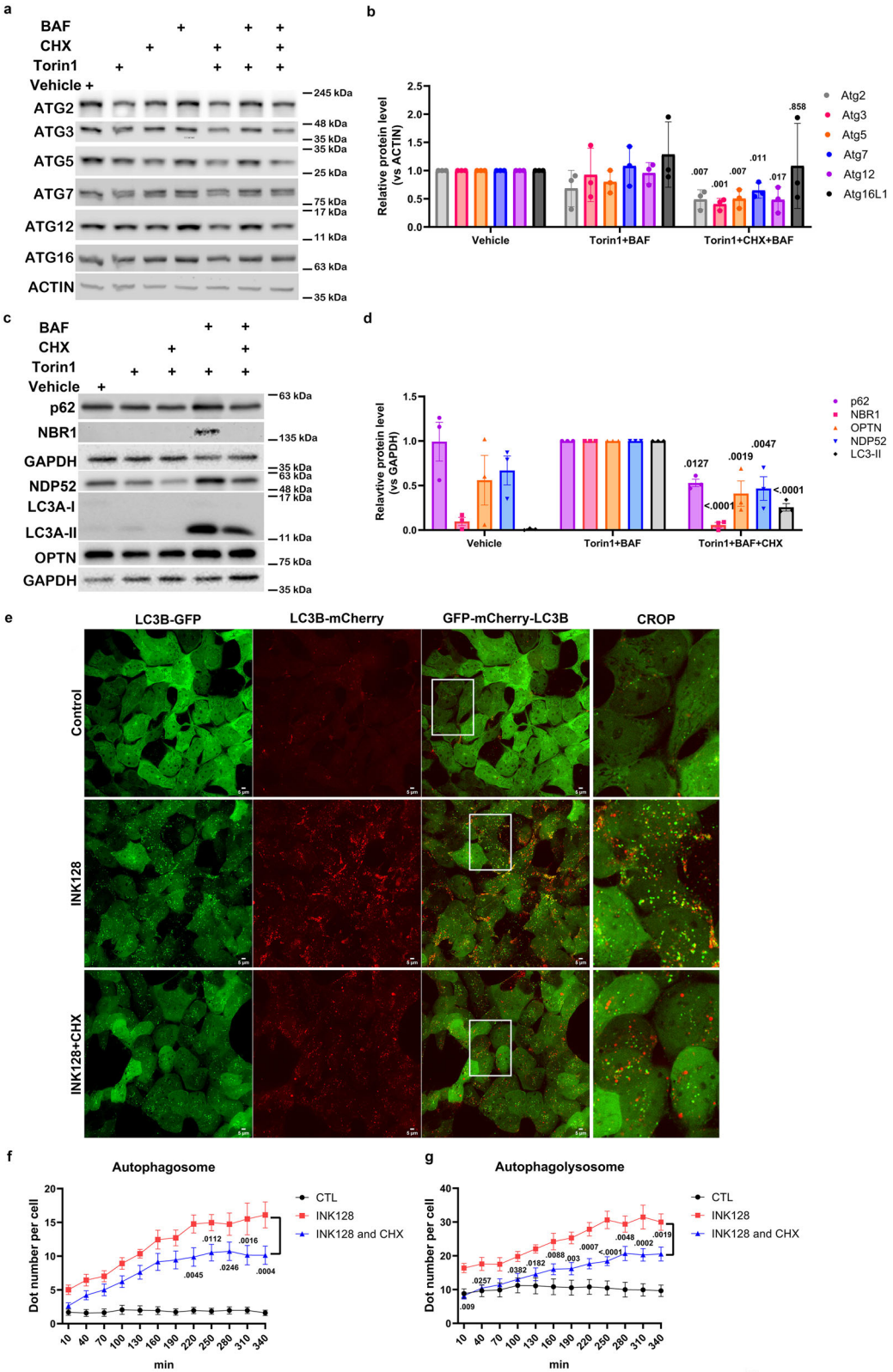

profiling (Supplementary Fig. 4e) and AHA nascent protein labeling (Supplementary Fig. 4f). However, consistent with the enrichment of RACK1 at phagophores (Fig. 5c, Supplementary Fig. 3i, j), RACK1 knockdown selectively had a more profound effect on translation in proximity to APEX2-DFCP1, even when this was normalized to account for its effect on global translation (input AHA-labeled proteins) and APEX2-DFCP1 pulldowns (Supplementary Fig. 4f). RACK1 knockdown also reduced levels of *ATG3*, *DFCP1* and *VPS34* mRNAs in heavy polysome fractions in proximity to DFCP1 (Fig. 6a). Cumulatively, this data demonstrates that RACK1 localizes to forming autophagosomes and preferentially controls translation of mRNAs encoding proteins required for autophagy there.

If the recruitment of mRNAs encoding proteins that are required for autophagy to the early phagophore is critical for sustained

Fig. 4 | Translation is required for sustained autophagy. a Western blots of ATG2, ATG3, ATG5, ATG7, ATG12, ATG16L1, and β-actin proteins of cells untreated or treated with Torin1 (250 nM), ±BAF (500 nM), ±CHX (100 μg/mL) for 6 h. **b** Quantification of ATG2, ATG3, ATG5, ATG7, ATG12, ATG16L1, and β-actin levels of blots (**a**). Significance was calculated by comparing to Torin1+BAF group using Two-way ANOVA analysis. Data are expressed as mean ± SD ($n = 3$ biological replicates). **c** Western blots of p62/SQSTM, NBR1, NDP52, OPTN, LC3A-II and GAPDH proteins from cells untreated or treated with ±Torin1 (250 nM), ±BAF (500 nM), or ±CHX (100 μg/mL) for 6 h. **d** Quantification of proteins of blots (**c**). Significance was calculated by comparing to Torin1+BAF group with Two-way ANOVA analysis. Data are expressed as mean ± SEM ($n = 3$ biological replicates). **e** Representative microscopy images of HEK293T cells stably expressing GFP-mCherry-LC3B untreated or treated with INK128 (50 nM) ± CHX (100 μg/mL) for 6 h, and the quantification of autophagosomes (**f**) and autophagolysosomes (**g**). The number of dots per cell was quantified from ≥6 images (> 250 cells per time point). Data are presented as mean ± SEM and were analyzed using two-way ANOVA.

autophagy, then depleting RACK1 should decrease the rate of autophagy. Similar to cycloheximide treatment, RACK1 knockdown significantly decreased the protein level of p62/SQSTM, LC3A/B-II, NBR1, ATG3, ATG5-ATG12, VPS34, and OPTN many of which are required for autophagic degradation (Fig. 6b–j). While DFCP1 and NDP52 protein levels appeared to decrease after RACK1 knockdown, this did not reach statistical significance (Fig. 6f, j). RACK1 knockdown significantly inhibited autophagosome and autolysosome formation, as measured using the LC3B-GFP-mCherry system (Supplementary Fig. 4g and Fig. 6k, l), and again the reduction of autophagosomes and autophagolysosomes was not caused by a fluorescence intensity change of GFP (Supplementary Fig. 4h) and mCherry (Supplementary Fig. 4i).

RACK1 associates with an autophagosome biogenesis complex (Atg14L-Beclin 1-Vps34-Vps15) upon its phosphorylation by AMPK at Thr50[58]. RACK1 also binds 40S ribosomes, and a R36D/K38E mutant of RACK1 inhibits this[65]. Thr50 and R36D/K38E mutants of RACK1 were generated and used to further dissect the mechanism by which RACK1 localizes mRNAs to phagophores. APEX2-DFCP1 expressing cells were co-transfected with RACK1 siRNAs targeting the 3'UTR of RACK1 and Flag-RACK1 mutants (Fig. 6m). Wild-type RACK1 rescued the recruitment of Atg mRNAs into proximity of DFCP1 (Fig. 6n). Either RACK1 mutant abrogated the enrichment of transcripts encoding autophagy proteins to DFCP1 (Fig. 6n) and inhibited the formation of autophagosomes (Fig. 6o). This indicates that interrupting RACK1 association with ribosomes or with phagophores impairs recruitment of these mRNAs to forming autophagosomes and autophagy.

Cumulatively, our data demonstrates that several mRNAs essential for autophagy preferentially localize in proximity to forming autophagosomes and were translated there in a RACK1-dependent manner. Local translation of these mRNAs in a RACK1-dependent manner is critical for sustaining levels of autophagy.

Discussion

The evidence provided here demonstrates using FISH and proximity-labeling that many mRNAs encoding proteins required for autophagy are enriched in proximity to forming autophagosomes compared to other mRNAs, including those encoding histones, mitochondrial proteins and β-Actin. These structures are likely phagophores, as they co-localize with phagophore markers like DFCP1 or WIPI2 and require FIP200. This may also explain why the enrichment of these mRNAs in proximity to DFCP1 was frequently higher than LC3B, which is present both at phagophores and in mature autophagosomes. Analyses by microscopy show that not every punctate structure with DFCP1, WIPI2, or WIPI1 co-localizes with these mRNAs. This could have several explanations. Some of these puncta may be proteins associated with ER or other membranes that are not currently involved in forming autophagosomes. Alternatively, recruitment of mRNAs and local translation could occur on a specific subset of forming autophagosomes or only at specific time points during autophagosome formation.

EM studies have suggested that ribosomes are not directly attached to the ER membranes which are incorporated into forming autophagosomes. Others have noted that ribosomes are apparent in the vicinity of forming autophagosomes[66–68]. This suggests the possibility of translationally competent ribosomes in proximity to forming autophagosomes that could furnish a rapid, local supply of key proteins involved in autophagosome biogenesis. Notably, the autophagy-related mRNAs and sites of translation frequently appear to be immediately adjacent to or partially overlapping with markers of forming autophagosomes. This is consistent with their being adjacent to omegasomes or phagophores and not directly on the ribosome-free membranes forming these.

Others have shown that ribosomes can be degraded by autophagy in both yeast and mammalian cells[30,69–72]. These studies used extended treatments with mTOR inhibitors or starvation (24–72 h) to observe ribophagy. Even after 24–72 h of mTOR inhibition, a comprehensive analysis demonstrated only a 3–4% reduction in levels of ribosomes due to ribophagy[71]. Ribophagy was undetectable prior to 10 h in all studies to our knowledge[31,71]. In contrast, our experiments analyzed cells after 2–4 h of mTOR inhibitor treatment when ribophagy is undetectable. Studies on ribophagy, to our knowledge, have not examined whether ribosomes degraded by autophagy are bound to mRNAs. The ribosomes degraded by autophagy are poly-ubiquitinated however, and are hypothesized to be damaged, inappropriately assembled, or non-functional[73]. In contrast, our data using fractionation of heavy polysomes, Click-iT, and SILAC labeling of nascent translation suggest that mRNAs encoding proteins involved in autophagy are selectively translated in proximity to forming autophagosomes. It is possible that ribosomes may localize to phagophores for degradation. However, such ribosomes would not be expected to be selectively enriched in mRNAs encoding autophagy-related proteins, which are included in heavy polysomes and producing nascent ATG3, ATG5, p62, DFCP1, and VPS34 as our data shows. According to the model proposed by the Harper lab[71], ribophagy occurs as a non-selective bystander process, and thus would not preferentially recruit mRNAs involved in autophagy. Our work suggests that ribosomes involved in translating mRNAs in proximity to forming autophagosomes escape engulfment and degradation. Mechanisms which position these ribosomes on proximal membranes or the exterior surface of phagophores could enable these ribosomes to better escape degradation.

mRNAs encoding proteins involved in cell division were also enriched in proximity to DFCP1 and phagophores. Translation of these mRNAs was not detected by nascent peptide proteomics. Inhibition of mTOR inhibits cell growth and cell division. This pool of mRNAs may localize in proximity to DFCP1 for post-transcriptional repression, or potentially for degradation by autophagy.

Data presented here demonstrates that localization of autophagy-related mRNAs to forming autophagosomes is dependent on RACK1. Previous reports showed that RACK1 promotes autophagy[74] and serves as a scaffold for the VPS34-PI3K complex and Atg14 to regulate phagophore initiation[58]. This places RACK1 at the forming autophagosome and suggests it can regulate autophagy. RACK1 can also bind to 40S ribosomes and regulate translation. RACK1 does not appear to be a constitutive member of the 40S ribosome, and it regulates translation of selective sets of mRNAs[59], including shorter mRNAs and those undergoing m^7g Cap-independent translation[60,75]. In neurons, RACK1 has been documented to regulate mRNA localization and local translation by associating with other RNA-binding proteins[76,77]. Our data suggest that mRNA localization and local translation at forming autophagosomes is dependent on RACK1. This capacity of RACK1 may involve an association of RACK1 with other RNA-binding proteins or

https://doi.org/10.1038/s41467-026-71551-4

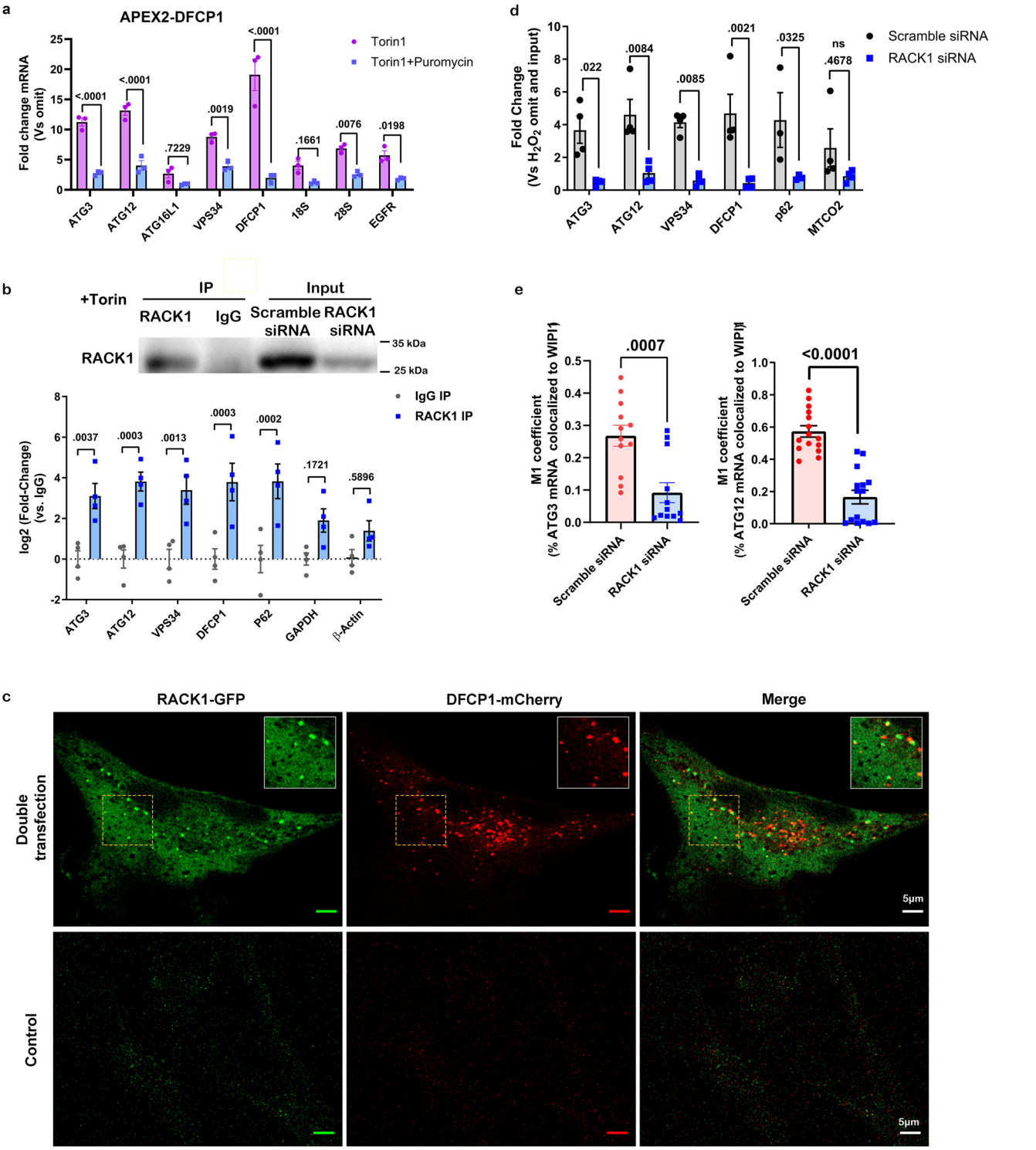

Fig. 5 | RACK1 controls localization of autophagy-related mRNAs in proximity to forming autophagosomes. a RT-qPCR analysis of APEX2-DFCP1 proximity-labeling pulldowns showing specific enrichment of Atg mRNAs in proximity to DFCP1 was inhibited by puromycin treatment. Cells were treated with Torin1 (250 nM, 4 h) ± puromycin (100 μg/mL, 1 h) before being labeled with BP ± H_2O_2. Data are expressed as mean ± SEM and were analyzed using two-way ANOVA ($n = 3$ biological replicates). **b** Western blot of RACK1 in immunoprecipitation using RACK1 antibody and RT-qPCR of several mRNAs co-immunoprecipitated by RACK1 antibody. Data are expressed as mean ± SEM and were analyzed using two-way ANOVA ($n = 4$ biological replicates). GAPDH, $p = 0.1721$ and β-actin, $p = 0.5896$. **c** Fluorescence microscopy of cells co-transfected with RACK1-GFP and DFCP1-mCherry plasmids and treated with Torin1. **d** RACK1 knockdown abrogated the recruitment of several Atg mRNAs to DFCP1. RT-qPCR of APEX2-DFCP1 labeled RNA from cells transfected with RACK1 or scramble siRNAs and treated with Torin1 (250 nM, 4 h). Data are expressed as mean ± SEM and were analyzed using two-way ANOVA ($n = 4$ biological replicates). **e** Quantification of co-localization (M1 colocalization co-efficient) of *ATG3* mRNA or *ATG12* mRNA (FISH) and WIPI1-GFP in cells transfected with siRNA targeting *RACK1* or scramble siRNAs. Data represent $n > 12$ images obtained from three independent experiments (>40 cells in total were quantified), and statistical significance was determined using a t-test (two-sided). Data are expressed as mean ± SEM.

https://doi.org/10.1038/s41467-026-71551-4

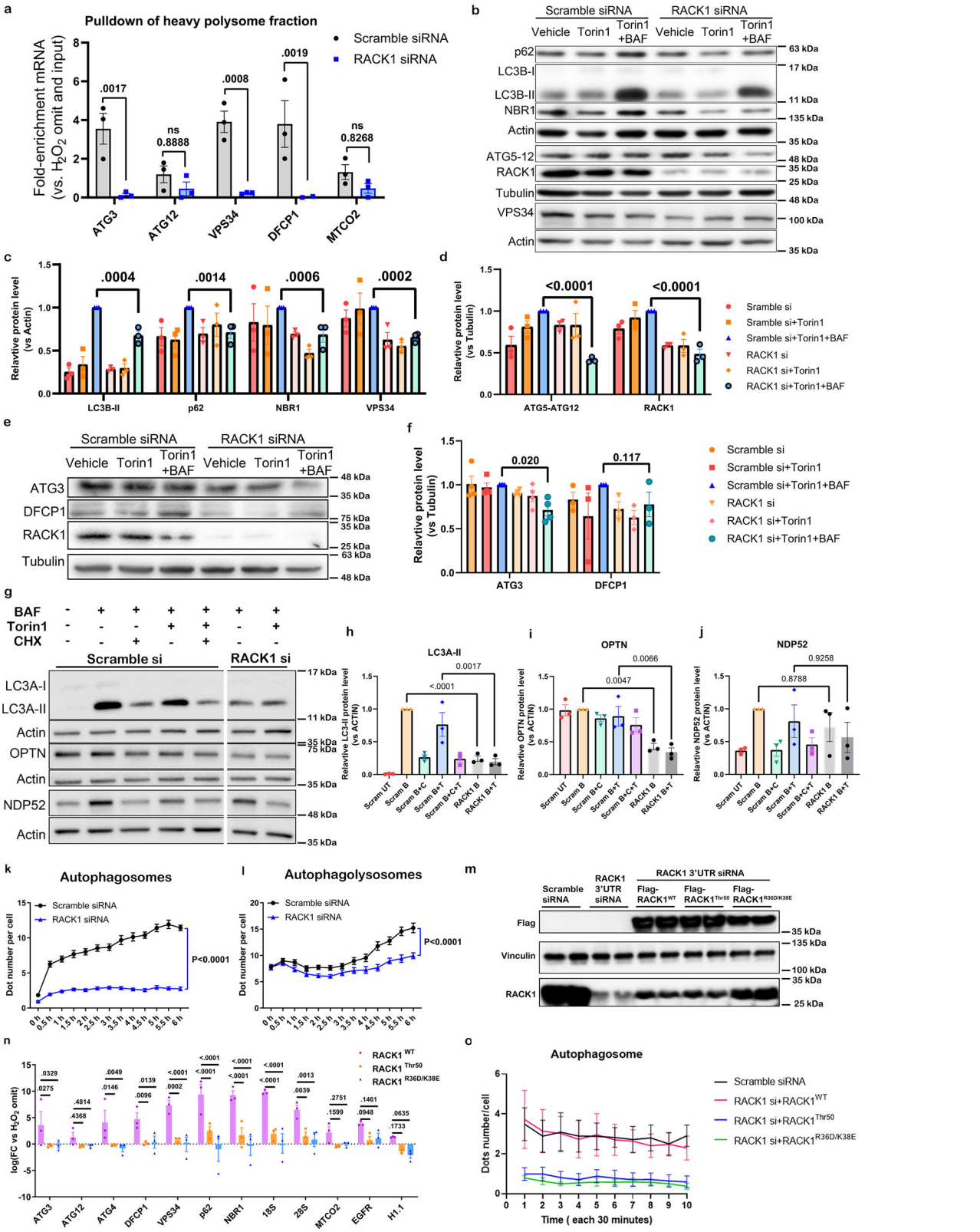

specific subsets of ribosomes through unidentified factors. Localization of mRNA into the proximity of forming autophagosomes was also dependent on binding of ribosomes to mRNA, as it was reduced by puromycin treatment. This suggests recruitment of mRNAs to forming autophagosomes may require marking of specific ribosomes by RACK1. This is another example of mRNA localization which requires ongoing translation[8] beyond the example of co-translational targeting of mRNAs encoding transmembrane and secreted proteins to the rough ER.

mRNAs required for autophagy continue to be translated when global translation is decreased during stress. This process required RACK1, but additional factors may also help promote localization and translation of mRNAs encoding proteins involved in autophagy. Several post-transcriptional mechanisms control translation of these

Fig. 6 | RACK1 regulates translation of proteins required for autophagy in proximity to phagophores. a RT-qPCR quantification of mRNA in heavy polysome fractions from HeLa cells transfected with indicated siRNAs and treated with Torin1. Data are presented as mean ± SEM and analyzed by two-way ANOVA ($n = 3$ biological replicates). **b**, **e**, **g** Western blot of proteins involved in autophagy in cells transfected with siRNA targeting *RACK1* or scramble siRNA and their quantification (**c**, **d**, **f**, **h**, **i**, **j**). B=BAF, T=Torin1. Data are presented as mean ± SEM ($n = 3$ biological replicates) and analyzed by two-way ANOVA followed by Sidak's multiple comparisons test (two-sided). All displayed separated protein bands of different groups in (**g**) were on the same PVDF membrane. Quantification of autophagosome (**k**) and autophagolysosome (**l**) formation in HEK293 cells expressing GFP-mCherry-LC3B and transfected with scramble siRNAs or *RACK1* targeting siRNAs. The number of dots per cell was quantified (>500 cells per time point from ≥11 images). Data are presented as mean ± SEM and were analyzed using two-way ANOVA. **m** Western Blot of RACK1 knockdown by siRNA targeting RACK1 3′UTR and overexpression of Flag- RACK1^{Thr50} or RACK1$^{R36D/K38E}$. **n** RACK1^{Thr50} and RACK1$^{R36D/K38E}$ mutants abrogated the recruitment of several Atg mRNAs to DFCP1. RT-qPCR of APEX2-DFCP1 biotinylated RNAs from APEX2-DFCP1 expressing cells co-transfected with RACK1 3′UTR siRNAs and plasmids (Flag-RACK1^{Thr50}, Flag-RACK1$^{R36D/K38E}$, or Flag-RACK1^{WT}) under Torin1 treatment. Data are presented as mean ± SEM and analyzed by two-way ANOVA ($n = 3$ biological replicates). **o** Quantification of autophagosomes in GFP-mCherry-LC3B expressing cells co-transfected with RACK1 3′UTR siRNA and plasmids (Flag-RACK1^{Thr50}, Flag-RACK1$^{R36D/K38E}$, or Flag-RACK1^{WT}) under Torin1 treatment for 5 h. The number of dots per cell was quantified from 4 images and data are presented as mean ± SEM.

mRNAs, for example, involving eIF5a[78], microRNAs, and the RNA-binding protein HuR[79]. eIF5A regulates translation of ATG3 and p62, but this was dependent on a polyproline sequence not found in many of the mRNAs detected in proximity to phagophores[78]. A sequence or structure could recruit mRNAs to the phagophore.

One candidate protein that may work with RACK1 to control local translation of mRNAs is EIF3D. When mTOR is inhibited EIF4E-dependent translation is greatly diminished. EIF3D can bind to the 5′ cap of mRNA and the 40S ribosomal subunit to initiate translation of a selective set of mRNAs independent of EIF4E[80]. EIF3D has been identified to allow and induce translation when EIF4E-dependent translation was blocked by mTOR inhibition[81]. Notably, a recent paper suggested that RACK1 may help control EIF3D-dependent translation[82]. This suggests that RACK1 and EIF3D may help localize and regulate the translation of mRNAs at forming autophagosomes.

Co-translational recruitment of mRNAs by nascent proteins could also explain the enrichment of mRNAs encoding proteins involved in autophagy in proximity to phagophores. mRNAs were detected in heavy polysomes in proximity to phagophores, which means as one ribosome initiates translation, others may be midway through the coding sequence or nearing the stop codon. Nascent proteins begin to fold as they emerge from the ribosome, and these could bind mature proteins which localize to phagophores, recruiting polysome-associated mRNAs with them. Similar processes have been observed now at multiple sites, including mitochondria[83] endosomes[8] and nuclear pores[84].

Our evidence suggests that mRNAs encoding proteins required for autophagy localize in proximity to forming autophagosomes and are translated there. Large proportions of mRNAs in cells localize to the sites where their encoded proteins are necessary[85]. This is hypothesized to conserve cellular energy and provide a rapid local supply of the required proteins. Local translation may empower cells in the midst of stress responses to rapidly form autophagosomes while conserving energy.

Methods

Cell culture

HeLa (CCL2, ATCC) and HEK293T (CRL-3216, ATCC) cells were cultured in complete medium (Dulbecco's Modified Eagle's Medium containing 10% fetal bovine serum and 1% penicillin-streptomycin) in the incubator at 37 °C with 5% CO_2. Details of all reagents, equipment, and cell lines used in this study are provided in Table 1.

In vitro APEX2 proximity labeling

APEX2-DFCP1 plasmid, APEX2-DFCP1 and -LC3B expressing Hela cells were generated by Dr. Christian Behrends' lab[37]. APEX2 expressing cells were seeded on 15 cm plates until they were 90% confluent. Twenty-four hours before collection, APEX2 expression was induced with doxycycline (40 μg/mL). On the day of collection, cells were treated with Torin1 to induce autophagy. APEX2 labeling was then initiated by changing the medium to fresh DMEM medium containing 500 mM (Biotin-Phenol/ biotin-tyramide) BP and Torin1. The cells were incubated at 37 °C under 5% CO_2 for 30 min, followed by gentle agitation for one min after the addition of 1 mM H_2O_2. The unlabeled controls were processed identically, except that the H_2O_2 addition step was omitted.

The APEX2 reaction was quenched by replacing the medium with an equal volume of quenching buffer (5 mM Trolox, 10 mM sodium ascorbate, and 10 mM sodium azide in DPBS) and gently agitating for 10 min. Cells were further washed with cold PBS twice, scraped with cell lifters, and transferred to 1.5-mL Eppendorf tubes. The cells were pelleted by centrifugation at 300 × g for 3 min at 4 °C and stored at −80 °C for further experiments.

Streptavidin purification of biotinylated RNAs

TRIzol was added to APEX2 proximity biotinylated or unlabeled (controls) cell pellets. The cellular RNAs were extracted following the Tri-Reagent isolation protocol. Dynabeads™ MyOne™ Streptavidin C1 Beads were used to enrich biotinylated RNAs. Ten microliters beads were used for every 25 μg of total RNA. Beads were pre-washed with 1×Binding and Washing (B & W) Buffer (5 mM Tris-HCl (pH 7.5), 0.5 mM EDTA, and 1 M NaCl) three times, followed by two washes with Solution A (DEPC-treated 0.1 M NaOH and DEPC-treated 0.05 M NaCl), and one wash with Solution B (DEPC-treated 0.1 M NaCl). The beads were then suspended in 500 μL of 2× B & W Buffer and incubated with above RNAs, dissolved in 500 μL of water on a rotator for 2 h at 4 °C. After rotation, beads were washed with 1× B & W Buffer on a magnet rack three times. The beads were resuspended in 7 μL RNase-free water for downstream RT-qPCR applications.

RT-qPCR on biotinylated RNAs

Ten microliters M-MuLV Reverse Transcriptase Reaction system was used to syntheses cDNA from input RNAs (1 μg) or captured biotinylated RNAs on beads. After reverse transcription, the cDNA was separated from the beads using a magnet. The cDNA was diluted 10 times for qPCR. Custom primers (Table 2 below) were ordered from IDT. The SYBR™ Green Master Mix was used for qPCR as follows: 95 °C for 2 min, (95 °C for 30 s, 55 °C (vary with primers) for 30 s, 72 °C for 45 s) × 50 cycles, 72 °C for 10 min.

APEX2-seq

APEX2 biotinylated RNAs were pulled down by streptavidin beads and purified with TRIzol before being sent to sequencing service provider Innomics for RNA sequencing with the DNBSEQ platform with paired-end read lengths of 100 bp. RNA-seq libraries were constructed following the Standard DNBSEQ Eukaryotic Transcriptome Resequencing protocols.

The raw data from the DNBSEQ platform was processed using nf-core/rnaseq v3.14.0 (https://doi.org/10.5281/zenodo.1400710) of the nf-core collection of workflows[86]. Sequences were aligned to the human GRCh38 genome and v45 GENCODE annotations using STAR

Table 2 | Primer sequences

Primer name	Sequence
ATG3-F	ACTGGAAGTGGCTGAGTACC
ATG3-R	CTGTAGCCCATTGCCATGTTG
ATG12-F	CTATGAGTGTTTTGGCAGTGATGG
ATG12-R	TTCAGAGCTGTCTCTTCCGTG
ATG16L1-F	CGAGAGATGGAGCTGTTGGG
ATG16L1-R	CCCAGGTGCACTGAATGTCT
VPS34-F	CATGTTTCGCCAAGGGATGC
VPS34-R	TGGTGAGCTTGGCAAGACG
DFCP1-F	CTTCATGGCTCAGTCGGTGT
DFCP1-R	TGCAGCTCAGAATCTGGGAG
18s-F	GTTCAGCCACCCGAGATTGA
18s-R	CCCATCACGAATGGGGTTCA
28s-F	AGCCGACTTAGAACTGGTGC
28s-R	GGCAGAAATCACATCGCGTC
MAP1LC3B/B2-F	GAGAAGCAGCTTCCTGTTCTGG
MAP1LC3B/B2-R	GTGTCCGTTCACCAACAGGAAG
MTCO2-F	AACCAAACCACTTTCACCGC
MTCO2-R	CGATGGGCATGAAACTGTGG
EGFR-F	TTGCCGCAAAGTGTGTAACG
EGFR-R	GAGATCGCCACTGATGGAGG
H1.1-F	AGGCAACGGGTGCATCTAAA
H1.1-R	GATTTCCTTGTTGCCGCAGG
ATG7-F	CGTTGCCCACAGCATCATCTTC
ATG7-R	CACTGAGGTTCACCATCCTTGG
ATG5-F	GCAGATGGACAGTTGCACACAC
ATG5-R	GAGGTGTTTCCAACATTGGCTCA
ATG2B-F	CTTCAGATGGAGTTGGAGGAGAC
ATG2B-R	AGTGGCTCCTTTCAGTCCTACG
p62-F	TGTGTAGCGTCTGCGAGGGAAA
p62-R	AGTGTCCGTGTTTCACCTTCCG
ATG4-F	CCTTCGCCTGGGCATAAA
ATG4-R	GTATGAGGGTCCAAGAAGATGAG
NBR1-F	CCTGAGAGCTTGCTCCAGTCTA
NBR1-R	CTTGGTTCCTGGCTGAAGGTGA
NDP52-F	CCAGTTCTGCTATGTGGATGAGG
NDP52-R	GTGCTGCTCAATCTCTTCCACC
RACK1-F	AATACCCTGGGTGTGTGCAA
RACK1-R	GCCAGGTTCCATACCTTGACC

2.7.9a[87] and quantified using Salmon 1.10.1[88], generating gene based read counts and TPM files. Limma-Voom was used to quantify the adjusted P-value and fold change of genes between H_2O_2 groups and omit conditions from APEX2-DFCP1, -Cyto-V5, and -Perilipin groups. The dot plot showing fold-change and adjusted P-value was generated.

Immunofluorescence

Cells were seeded on cover slips. On the day of collection, cover slips were fixed with 1% PFA (paraformaldehyde) for 10 min at RT and washed with PBS three times. Fixed cells were permeabilized with permeabilization buffer (20 mM NH_4Cl, and 0.2% Triton in PBS) for 30 min at RT. Cells were subsequently blocked with 1% BSA for 1 h before incubating with primary antibody overnight at 4 °C. The next day, coverslips were washed with PBS and incubated with fluorophore-tagged secondary antibody for 1 h at RT. Coverslips were then washed with PBS and mounted on slides with VECTASHIELD mounting medium.

Polysome fractionation

APEX2 expressing cells were processed through proximity labeling as previously described. The cells were treated with 100 μg/μL of CHX for 5-10 min before applying quenching buffer. The cells were scraped and pelleted at 400 × *g* at 4 °C. Cell Pellets were resuspended in 450 μL of the 1st lysis buffer (5 mM Tris-HCl pH 7.5, 1.5 mM KCl, 2.5 mM $MgCl_2$, 1× Protease Inhibitor, 20 U/mL RNAse Inhibitor, 1 mM DTT, and prepared in RNAse-free conditions) and vortexed for 5 s. Fifty microliters of the 2nd lysis buffer (0.5% Triton X-100, 0.5% Sodium deoxycholate) were subsequently added to the cell suspension which was then vortexed for 5 s. The cells in lysis buffer were incubated on ice for 15 min. Cell lysate was collected by pelleting cell debris at 14,000 rpm at 4 °C for 15 min. Absorbance at 260 nm was used to normalize sample amounts in 500 μL. Ten percent of lysate samples (50 μL) was kept in −80 °C as input. 60% (w/v) sucrose was diluted in polysome buffer containing 20 mM HEPES (pH 7.6), 0.1 M KCl, 5 mM $MgCl_2$, 1× Protease Inhibitor, 20 U/mL RNAse Inhibitor, 0.1 mM DTT, and prepared in RNAse-free conditions to make 5% (w/v) and 50% (w/v) sucrose solutions. Sucrose gradients were prepared with the BioComp model 108 Gradient Master. Five hundred μL were removed from the top of each sucrose gradient and 450 μL of cell lysate samples were slowly loaded on top to prevent disrupting the gradient. The tubes were balanced using hypotonic lysis buffer before centrifugation at 39,000 rpm at 4 °C for 2 h with an SW41Ti rotor. After centrifugation, sucrose gradients were fractionated into ribosome-free sub-polysome fractions (sub), light polysome fractions (light) and heavy polysome fractions (heavy) using a density gradient fractionation system by monitoring their absorbance at 254 nm. The separated sucrose gradient fractions were stored at −80 °C prior to further processing.

Streptavidin purification of biotinylated RNAs from different ribosome fractions

1.8 mL of 2 mL of sucrose samples (containing RNAs and proteins) from ribosome-free sub fractions, light polysome fractions or heavy polysome fractions were incubated with 5–10 μL of MyOne™ Streptavidin C1 beads and rotated for 2 h at 4 °C. The leftover 0.2 mL of sucrose was used as input. Biotinylated samples coated with Streptavidin C1 beads were then washed with 1× B &W Buffer and washed with a magnet three times. TRIzol was then added to the input samples and beads to purify biotinylated RNAs for RT-qPCR.

FISH staining

Cells were seeded on glass coverslips and transfected with plasmid for 48 h. Cells were fixed in 4% PFA in PBS for 10 min at room temperature (RT) and washed with PBS, the slides were subsequently permeabilized and blocked for 1 h at RT with (0.2% Triton X-100, 1% BSA, 100 μg/mL salmon sperm DNA, and 250 μg/mL yeast extract RNA in PBS). Slides were washed with Stellaris Wash Buffer A at RT. Stellaris fluorescent mRNA probes (*ATG3*, *ATG12*, and *β-actin*) were placed in hybridization buffer (90% Stellaris Hybridization buffer, 10% formamide) and incubated with cells in the dark at 37 °C overnight. Slides were washed with Wash Buffer A, mounted with VECTASHIELD mounting medium with DAPI and sealed with nail polish.

Streptavidin purification of APEX2 biotinylated nascent proteins

APEX2-DFCP1 expressing cells cultured in methionine-free RPMI medium with Torin1 were treated with or without AHA (50 μM) for 30 min before APEX2-DFCP1 proximity labeling. Cells were washed two times with PBS, scraped with cell lifters, and transferred to 1.5-mL Eppendorf tubes and pelleted. Cell pellets were lysed with 50–100 μL of the lysis buffer (0.5% sodium deoxycholate, 0.5% Triton X-100 in PBS) before centrifugation at 10,000 × *g* for 15 min. Biotinylated proteins in the supernatant were clicked to Alexa Fluor™ 488 Alkyne (5 μM) using the Click-iT® Protein Reaction Buffer Kit. APEX2 biotinylated

proteins were pulled down with Streptavidin C1 beads for Western blot and detected with HRP-conjugated anti-Alexa488.

SILAC labeling and sample preparation for mass spectrometry

APEX2-DFCP1 expressing cells were incubated in Torin1 containing DMEM consisting of 13C6 15 N2 L-Lysine-2HCl and 13C6 15 N4 L-Arginine-HCl for 30 min, before being biotinylated with BP and H_2O_2, and lysed with RIPA buffer followed by streptavidin beads pulldown. For 100% labeling. Cells were incubated in DMEM consisting of 13C6 15 N2 L-Lysine-2HCl and 13C6 15 N4 L-Arginine-HCl and passaged for five doubling events, and the incorporation of heavy amino acids was tested using mass spectrometry analysis.

Biotin-streptavidin pulldown samples were prepared for mass spectrometry analysis with an on-bead digestion method. Briefly, a magnetic stand was used to remove liquid from the beads. And beads were resuspended in 9 μL of 20 mM Tris-HCl (pH 8) with 1.6 μL of 25 mM DTT, then incubated for 30 min at room temperature. After adding 1.2 μL of 50 mM iodoacetamide and incubating for 10 min, 10 μL of 100 ng/μL mass-spec grade trypsin was then added to achieve a final concentration of 45 ng/μL. The mixture was then incubated on the rotator at 37 °C overnight. The next day, the beads were removed with a magnetic stand, and an additional 500 ng of trypsin was added for 4 h incubation at 37 °C with gentle vortexing. Digestion was stopped with formic acid (F.A.) at a final concentration of 2%. For desalting, Sep-Pak tc18 1cc cartridges were conditioned in 900 μL of 100% acetonitrile (ACN) followed by 300 μL of 50% ACN and 0.5% acetic acid (HAcO). Cartridges were then equilibrated with 900 μL of 0.1% trifluoroacetic acid (TFA). Samples were adjusted to a final concentration of 0.4% TFA, passed through the cartridges, desalting with 900 μL of 0.1% TFA, and washing with 90 μL of 0.5% HAcO and elution with 500 μL of 50% ACN, 0.5% HAcO.

The peak lists of all raw files were processed and analyzed with software MaxQuant (Version 1.6.17.0). against Swissprot protein database of Human (2012, July Release), including commonly observed contaminants. Cysteine carbamidomethylation was selected as a fixed modification; the methionine oxidation (+15.99492 Da), protein N-terminal acetylation. Enzyme specificity was set to trypsin, not allowing for cleavage N-terminal to proline. Up to two missing cleavages of trypsin were allowed. For SILAC-labeled samples, Arg10 and Lys8 were chosen as light and heavy labels with Multiplicity 2 for quantification. The precursor ion mass tolerances were 7 ppm, and fragment ion mass tolerance was 0.8 Da for MS/MS spectra. Razor and unique peptides were used for quantitation. FDR was set at 0.01 on both protein and peptide level. LCMS Analysis was processed by following this protocol[89] and generated data was recorded using Xcalibur software (ThermoFisher Scientific).

Live cell imaging

Cells were seeded on μ-Slide 8-well chambered polymer coverslips at a density of 15,000 cells per well. A live imaging chamber maintained at 5% CO_2 and 37 °C on a Quorum spinning disk confocal microscope (Leica DMI6000B inverted model) was used. Multiple cells in the field of view were selected for imaging and phenol-free DMEM medium containing INK128 (50 nM) with or without CHX (100 μg/mL) was added. Cells were imaged every 30 min for up to 6 h. DAPI signals (405 nm laser and DAPI emission filter set, 460/50 nm), GFP signals (490 nm laser and FITC emission filter set, 525/50 nm), and mCherry signals (561 nm laser and Cy3 emission filter set, 605/52 nm) were used. A 63X oil immersion objective/1.4 NA was used. Images were captured with a sCMOS camera: Photometrics Prime BSI (1966 × 1966).

Imaris software analysis

Colocalization of GFP and mCherry positive foci was analyzed by the distance between these using Imaris software. If the distance was less than or equal to the sum of half the diameter of GFP and mCherry foci these were defined as colocalized. Based on this, the software counted the number of single mCherry positive dots per cell and the number of double fluorescent dots (LC3-mCherry and LC3-GFP) per cell.

DNA plasmid transfection with Polyethylenimine (PEI)

Cells were rinsed with PBS and fresh complete medium was added. DNA was added to media without FBS and PEI (4 μL PEI to 1 μg plasmid DNA) was added. The mixture was incubated at room temperature for 15–30 min before adding it to the cell culture. Cells were used 48 h later.

Immunoprecipitation (IP)

Torin1 treated WT HeLa cells were lysed with NP40 lysis buffer (50 mM Tris-HCl pH 7.5, 150 mM NaCl, 1% NP40, 1 Roche Complete Protease Inhibitor Cocktail Tablet) for 20 min at 4 °C and centrifuged at 5000 × *g* for 10 min. Protein concentration was measured with a BCA assay. Ten μL of protein G-Dynabeads were added the lysate and rotated for 20 min at 4 °C to reduce non-specific binding to beads. One thousand μg pre-cleared lysate was then incubated with 4 μg RACK1 or mouse IgG antibody for 3 h at 4 °C before incubation with 25 μL wet volume of protein G-Dynabeads (1 h, 4 °C). Subsequently, beads were collected by using a magnetic rack and washed with 1 mL wash buffer (50 mM Tris-base, pH 7.5 and 150 mM NaCl, 0.1% NP-40) three times. Half of the samples were suspended in 1X SDS-sample buffer and boiled at 99 °C for 10 min and beads quickly removed using a magnet. Supernatants were used for Western blot. The remaining samples were used for RNA extraction and RT-qPCR.

RNA immuno-blot assay

Two microliters of APEX2 biotinylated RNAs and un-biotinylated RNAs were pipetted onto a positively charged nylon membrane (Roche, Mannheim, Germany). RNA was cross-linked to the membrane with UV light: 120 mJ for 1 min of both sides at 254 nm. Biotinylated RNAs were detected with Stabilized Streptavidin-Horseradish Peroxidase Conjugate and the Substrate Working Solution of Chemiluminescent Nucleic Acid Detection Module Kit and imaged with CCD camera.

Proximity ligation in situ assay

Duolink® In Situ Detection Reagents Orange kit (including Ligase, Ligation buffer, DNA polymerase, and Amplification Orange buffer) was used. Cells seeded on coverslips were fixed with 4% PFA and permeabilized before being blocked with Duolink Blocking buffer for 60 min at 37 °C. The coverslips were incubated with primary antibodies diluted in Duolink® Antibody Diluent for 1 h at room temperature. Coverslips were washed 2 times for 5 min in Wash Buffer A and then incubated with PLA probes MINUS and PLUS probes corresponding to the primary antibodies (Duolink® In Situ PLA Probe Anti-Mouse MINUS and Duolink® In Situ PLA Probe Anti-Rabbit PLUS) for 1 h at 37 °C. Then, coverslips were washed twice for 5 min with Wash Buffer A and then incubated with a DNA ligase diluted in Ligation buffer for 30 min at 37 °C. Coverslips were washed 2 times for 5 min with Wash Buffer A and incubated with a DNA polymerase diluted in Amplification buffer for 100 min at 37 °C. Finally, coverslips were washed 2 times for 10 min with Wash Buffer B and subsequent 0.01× Wash Buffer B for 1 min before being mounted with Duolink® In Situ Mounting Media with DAPI. Fluorescence was visualized with a Zeiss LSM800 confocal microscope.

siRNA transfection with Lipofectamine RNAiMAX

APEX2-DFCP1 expressing cells were transfected with siRNAs by Lipofectamine™ RNAimax as follows: cells were plated 1 day before transfection to be 50% confluent at the time of transfection. SiRNA-Lipofectamine™ RNAiMAX complexes were prepared in Opti-MEM and incubated for 5 min at room temperature. Plates were gently rocked to promote mixing, and cells were harvested 72 h later.

Lentiviral vector production and transduction

HEK293T cells stably expressing APEX2-DFCP1 were generated via lentiviral transduction. Lentivirus was produced through co-transfection of WT HEK293T cells with the packaging plasmids psPAX2 and pMD2.G, along with the APEX2-DFCP1 plasmid. The media was harvested 48 h and 72 h post-transfection and filtered through a 0.45 μM PES membrane. Lentivirus was concentrated by ultra-centrifuging media at 20,800 rpm with a 32Ti rotor for 2 h. HEK293T cells were seeded in 6-well plates 24 h before transduction with concentrated lentivirus promoted by 8 μg/mL of polybrene. After 48 h, media was changed, and cells were selected with puromycin (2 μg/mL).

Statistics and reproducibility

Statistical analyses were performed using GraphPad Prism version 8. Data are presented as mean ± SEM/mean ± SD unless otherwise indicated. Sample sizes were based on those generally used in the field for similar types of experiments. No data were excluded from the analyses. Plates were seeded from a single batch of cells and randomized to receive treatments. The experiments were not randomized.

Reporting summary

Further information on research design is available in the Nature Portfolio Reporting Summary linked to this article.

Data availability

All data are available in the main text and the source data file. Source data are provided with this paper. Gene Expression Omnibus (GEO) The RNA-seq data generated in this study have been deposited in the NCBI Gene Expression Omnibus (GEO) under accession code GSE319465. The protein mass spectrometry data generated in this study have been deposited in the PRIDE repository under accession code PXD073558 ("Proteomic analysis of nascent proteins in proximity to DFCP1 using SILAC labeling and APEX2-mediated biotin-streptavidin affinity purification.") and PXD073592 ("Proteomic analysis of RacK1 immunoprecipitates from Torin1-treated wild-type HeLa cells"). Source data are provided with this paper.

References

1. Das, S., Vera, M., Gandin, V., Singer, R. H. & Tutucci, E. Intracellular mRNA transport and localized translation. *Nat. Rev. Mol. Cell Biol.* **22**, 483–504 (2021).
2. Bourke, A. M., Schwarz, A. & Schuman, E. M. De-centralizing the central Dogma: mRNA translation in space and time. *Mol. Cell* **83**, 452–468 (2023).
3. Schwanhausser, B. et al. Corrigendum: Global quantification of mammalian gene expression control. *Nature* **495**, 126–127 (2013).
4. Huttelmaier, S. et al. Spatial regulation of beta-actin translation by Src-dependent phosphorylation of ZBP1. *Nature* **438**, 512–515 (2005).
5. Hegde, R. S. & Keenan, R. J. The mechanisms of integral membrane protein biogenesis. *Nat. Rev. Mol. Cell Biol.* **23**, 107–124 (2022).
6. Reid, D. W. & Nicchitta, C. V. Diversity and selectivity in mRNA translation on the endoplasmic reticulum. *Nat. Rev. Mol. Cell Biol.* **16**, 221–231 (2015).
7. Kloc, M., Zearfoss, N. R. & Etkin, L. D. Mechanisms of subcellular mRNA localization. *Cell* **108**, 533–544 (2002).
8. Chouaib, R. et al. A dual protein-mRNA localization screen reveals compartmentalized translation and widespread co-translational RNA targeting. *Dev. Cell* **54**, 773–791 e775 (2020).
9. Graber, T. E. et al. Reactivation of stalled polyribosomes in synaptic plasticity. *Proc. Natl. Acad. Sci. USA.* **110**, 16205–16210 (2013).
10. Filipovska, A. & Rackham, O. Specialization from synthesis: how ribosome diversity can customize protein function. *FEBS Lett.* **587**, 1189–1197 (2013).
11. Shi, Z. et al. Heterogeneous ribosomes preferentially translate distinct subpools of mRNAs genome-wide. *Mol. Cell* **67**, 71–83 e77 (2017).
12. Klann, K., Tascher, G. & Munch, C. Functional translatome proteomics reveal converging and dose-dependent regulation by mTORC1 and eIF2alpha. *Mol. Cell* **77**, 913–925 e914 (2020).
13. Chang, C., Jensen, L. E. & Hurley, J. H. Autophagosome biogenesis comes out of the black box. *Nat. Cell Biol.* **23**, 450–456 (2021).
14. Melia, T. J., Lystad, A. H. & Simonsen, A. Autophagosome biogenesis: from membrane growth to closure. *J Cell Biol.* **219**, e202002085 (2020).
15. Alers, S., Loffler, A. S., Wesselborg, S. & Stork, B. Role of AMPK-mTOR-Ulk1/2 in the regulation of autophagy: cross talk, shortcuts, and feedbacks. *Mol. Cell Biol.* **32**, 2–11 (2012).
16. Kim, J., Kundu, M., Viollet, B. & Guan, K. L. AMPK and mTOR regulate autophagy through direct phosphorylation of Ulk1. *Nat. Cell Biol.* **13**, 132–141 (2011).
17. Dikic, I. & Elazar, Z. Mechanism and medical implications of mammalian autophagy. *Nat. Rev. Mol. Cell Biol.* **19**, 349–364 (2018).
18. Axe, E. L. et al. Autophagosome formation from membrane compartments enriched in phosphatidylinositol 3-phosphate and dynamically connected to the endoplasmic reticulum. *J. Cell Biol.* **182**, 685–701 (2008).
19. Lamb, C. A., Yoshimori, T. & Tooze, S. A. The autophagosome: origins unknown, biogenesis complex. *Nat. Rev. Mol. Cell Biol.* **14**, 759–774 (2013).
20. Lamark, T. & Johansen, T. Mechanisms of selective autophagy. *Annu Rev. Cell Dev. Biol.* **37**, 143–169 (2021).
21. Bjorkoy, G. et al. p62/SQSTM1 forms protein aggregates degraded by autophagy and has a protective effect on huntingtin-induced cell death. *J. Cell Biol.* **171**, 603–614 (2005).
22. Johansen, T. & Lamark, T. Selective autophagy mediated by autophagic adapter proteins. *Autophagy* **7**, 279–296 (2011).
23. Klionsky, D. J. et al. Guidelines for the use and interpretation of assays for monitoring autophagy (4th edition)(1). *Autophagy* **17**, 1–382 (2021).
24. Biazik, J., Yla-Anttila, P., Vihinen, H., Jokitalo, E. & Eskelinen, E. L. Ultrastructural relationship of the phagophore with surrounding organelles. *Autophagy* **11**, 439–451 (2015).
25. Dunn, W. A. Jr Studies on the mechanisms of autophagy: maturation of the autophagic vacuole. *J. Cell Biol.* **110**, 1935–1945 (1990).
26. Dunn, W. A. Jr Studies on the mechanisms of autophagy: formation of the autophagic vacuole. *J. Cell Biol.* **110**, 1923–1933 (1990).
27. Ericsson, J. L. Studies on induced cellular autophagy. II. Characterization of the membranes bordering autophagosomes in parenchymal liver cells. *Exp. Cell Res.* **56**, 393–405 (1969).
28. Kishi-Itakura, C., Koyama-Honda, I., Itakura, E. & Mizushima, N. Ultrastructural analysis of autophagosome organization using mammalian autophagy-deficient cells. *J. Cell Sci.* **127**, 4089–4102 (2014).
29. Novikoff, A. B. & Shin, W. Y. Endoplasmic reticulum and autophagy in rat hepatocytes. *Proc. Natl. Acad. Sci. USA.* **75**, 5039–5042 (1978).
30. Kraft, C., Deplazes, A., Sohrmann, M. & Peter, M. Mature ribosomes are selectively degraded upon starvation by an autophagy pathway requiring the Ubp3p/Bre5p ubiquitin protease. *Nat. Cell Biol.* **10**, 602–610 (2008).
31. Wyant, G. A. et al. NUFIP1 is a ribosome receptor for starvation-induced ribophagy. *Science* **360**, 751–758 (2018).
32. Klionsky, D. J. et al. A comprehensive glossary of autophagy-related molecules and processes (2nd edition). *Autophagy* **7**, 1273–1294 (2011).
33. Voigt, F. et al. Single-molecule quantification of translation-dependent association of mrnas with the endoplasmic reticulum. *Cell Rep.* **21**, 3740–3753 (2017).

34. Pyhtila, B. et al. Signal sequence- and translation-independent mRNA localization to the endoplasmic reticulum. *RNA* **14**, 445–453 (2008).
35. Jagannathan, S., Reid, D. W., Cox, A. H. & Nicchitta, C. V. De novo translation initiation on membrane-bound ribosomes as a mechanism for localization of cytosolic protein mRNAs to the endoplasmic reticulum. *RNA* **20**, 1489–1498 (2014).
36. Fazal, F. M. et al. Atlas of subcellular RNA localization revealed by APEX-Seq. *Cell* **178**, 473–490 e426 (2019).
37. Le Guerroue, F. et al. Autophagosomal content profiling reveals an LC3C-dependent piecemeal mitophagy pathway. *Mol. Cell* **68**, 786–796 e786 (2017).
38. Feng, X. et al. Local membrane source gathering by p62 body drives autophagosome formation. *Nat. Commun.* **14**, 7338 (2023).
39. Kageyama, S. et al. p62/SQSTM1-droplet serves as a platform for autophagosome formation and anti-oxidative stress response. *Nat. Commun.* **12**, 16 (2021).
40. Wei, Y., Chiang, W. C., Sumpter, R. Jr., Mishra, P. & Levine, B. Prohibitin 2 is an inner mitochondrial membrane mitophagy receptor. *Cell* **168**, 224–238 e210 (2017).
41. Fielden, J., Popovic, M. & Ramadan, K. TEX264 at the intersection of autophagy and DNA repair. *Autophagy* **18**, 40–49 (2022).
42. Larsson, E., Moren, B., McMahon, K. A., Parton, R. G. & Lundmark, R. Dynamin2 functions as an accessory protein to reduce the rate of caveola internalization. *J Cell Biol.* **222** e202205122 (2023).
43. Zhou, C. et al. Recycling of autophagosomal components from autolysosomes by the recycler complex. *Nat. Cell Biol.* **24**, 497–512 (2022).
44. Nada, S. et al. The novel lipid raft adaptor p18 controls endosome dynamics by anchoring the MEK-ERK pathway to late endosomes. *EMBO J.* **28**, 477–489 (2009).
45. Zachari, M. & Ganley, I. G. The mammalian ULK1 complex and autophagy initiation. *Essays Biochem.* **61**, 585–596 (2017).
46. Hara, T. & Mizushima, N. Role of ULK-FIP200 complex in mammalian autophagy: FIP200, a counterpart of yeast Atg17? *Autophagy* **5**, 85–87 (2009).
47. Durgan, J. & Florey, O. Many roads lead to CASM: diverse stimuli of noncanonical autophagy share a unifying molecular mechanism. *Sci. Adv.* **8**, eabo1274 (2022).
48. Guo, H. et al. Atg5 disassociates the V(1)V(0)-ATPase to promote exosome production and tumor metastasis independent of canonical macroautophagy. *Dev. Cell* **43**, 716–730 e717 (2017).
49. Gardner, J. O., Leidal, A. M., Nguyen, T. A. & Debnath, J. LC3-dependent EV loading and secretion (LDELS) promotes TFRC (transferrin receptor) secretion via extracellular vesicles. *Autophagy* **19**, 1551–1561 (2023).
50. Ingolia, N. T., Ghaemmaghami, S., Newman, J. R. & Weissman, J. S. Genome-wide analysis in vivo of translation with nucleotide resolution using ribosome profiling. *Science* **324**, 218–223 (2009).
51. Ingolia, N. T., Lareau, L. F. & Weissman, J. S. Ribosome profiling of mouse embryonic stem cells reveals the complexity and dynamics of mammalian proteomes. *Cell* **147**, 789–802 (2011).
52. Pan, P. & van Breukelen, F. Preference of IRES-mediated initiation of translation during hibernation in golden-mantled ground squirrels, Spermophilus lateralis. *Am. J. Physiol. Regul. Integr. Comp. Physiol.* **301**, R370–R377 (2011).
53. Watanabe-Asano, T., Kuma, A. & Mizushima, N. Cycloheximide inhibits starvation-induced autophagy through mTORC1 activation. *Biochem. Biophys. Res. Commun.* **445**, 334–339 (2014).
54. Mizushima, N., Yoshimori, T. & Levine, B. Methods in mammalian autophagy research. *Cell* **140**, 313–326 (2010).
55. Latallo, M. J. et al. Single-molecule imaging reveals distinct elongation and frameshifting dynamics between frames of expanded RNA repeats in C9ORF72-ALS/FTD. *Nat. Commun.* **14**, 5581 (2023).
56. Fresno, M., Jimenez, A. & Vazquez, D. Inhibition of translation in eukaryotic systems by harringtonine. *Eur. J. Biochem.* **72**, 323–330 (1977).
57. Sengupta, J. et al. Identification of the versatile scaffold protein RACK1 on the eukaryotic ribosome by cryo-EM. *Nat. Struct. Mol. Biol.* **11**, 957–962 (2004).
58. Zhao, Y. et al. RACK1 Promotes Autophagy by Enhancing the Atg14L-Beclin 1-Vps34-Vps15 Complex Formation upon Phosphorylation by AMPK. *Cell Rep.* **13**, 1407–1417 (2015).
59. Kim, H. D., Kong, E., Kim, Y., Chang, J. S. & Kim, J. RACK1 depletion in the ribosome induces selective translation for non-canonical autophagy. *Cell Death Dis.* **8**, e2800 (2017).
60. Thompson, M. K., Rojas-Duran, M. F., Gangaramani, P. & Gilbert, W. V. The ribosomal protein Asc1/RACK1 is required for efficient translation of short mRNAs. *Elife* **5**, e11154 (2016).
61. Bai, Y., Zhou, K. & Doudna, J. A. Hepatitis C virus 3'UTR regulates viral translation through direct interactions with the host translation machinery. *Nucleic Acids Res.* **41**, 7861–7874 (2013).
62. Lee, J. S. et al. RACK1 mediates rewiring of intracellular networks induced by hepatitis C virus infection. *PLoS Pathog.* **15**, e1008021 (2019).
63. Johnson, A. G. et al. RACK1 on and off the ribosome. *RNA* **25**, 881–895 (2019).
64. Coyle, S. M., Gilbert, W. V. & Doudna, J. A. Direct link between RACK1 function and localization at the ribosome in vivo. *Mol. Cell Biol.* **29**, 1626–1634 (2009).
65. Gallo, S. et al. RACK1 specifically regulates translation through its binding to ribosomes. *Mol. Cell Biol.* **38**, e00230-18 (2018).
66. Yla-Anttila, P., Vihinen, H., Jokitalo, E. & Eskelinen, E. L. 3D tomography reveals connections between the phagophore and endoplasmic reticulum. *Autophagy* **5**, 1180–1185 (2009).
67. Dunkle, J. A. & Cate, J. H. Ribosome structure and dynamics during translocation and termination. *Annu Rev. Biophys.* **39**, 227–244 (2010).
68. Eskelinen, E. L., Reggiori, F., Baba, M., Kovacs, A. L. & Seglen, P. O. Seeing is believing: the impact of electron microscopy on autophagy research. *Autophagy* **7**, 935–956 (2011).
69. Bassham, D. C. & MacIntosh, G. C. Degradation of cytosolic ribosomes by autophagy-related pathways. *Plant Sci.* **262**, 169–174 (2017).
70. An, H. & Harper, J. W. Ribosome abundance control via the ubiquitin-proteasome system and autophagy. *J. Mol. Biol.* **432**, 170–184 (2020).
71. An, H., Ordureau, A., Korner, M., Paulo, J. A. & Harper, J. W. Systematic quantitative analysis of ribosome inventory during nutrient stress. *Nature* **583**, 303–309 (2020).
72. Lopez, A. R. et al. Autophagy-mediated control of ribosome homeostasis in oncogene-induced senescence. *Cell Rep.* **42**, 113381 (2023).
73. Frankel, L. B., Lubas, M. & Lund, A. H. Emerging connections between RNA and autophagy. *Autophagy* **13**, 3–23 (2017).
74. Erbil, S. et al. RACK1 is an interaction partner of ATG5 and a novel regulator of autophagy. *J. Biol. Chem.* **291**, 16753–16765 (2016).
75. Rollins, M. G. et al. Negative charge in the RACK1 loop broadens the translational capacity of the human ribosome. *Cell Rep.* **36**, 109663 (2021).
76. Kershner, L. & Welshhans, K. RACK1 is necessary for the formation of point contacts and regulates axon growth. *Dev. Neurobiol.* **77**, 1038–1056 (2017).
77. Romano, N. et al. Ribosomal RACK1 regulates the dendritic arborization by repressing FMRP activity. *Int. J. Mol. Sci.* **23**, 11857 (2022).
78. Lubas, M.et al. eIF5A is required for autophagy by mediating ATG3 translation. *EMBO Rep.* **19**, e46072 (2018).

79. Pullmann, R. Jr et al. Analysis of turnover and translation regulatory RNA-binding protein expression through binding to cognate mRNAs. *Mol. Cell Biol.* **27**, 6265–6278 (2007).
80. Lee, A. S., Kranzusch, P. J. & Cate, J. H. eIF3 targets cell-proliferation messenger RNAs for translational activation or repression. *Nature* **522**, 111–114 (2015).
81. Shin, S. et al. mTOR inhibition reprograms cellular proteostasis by regulating eIF3D-mediated selective mRNA translation and promotes cell phenotype switching. *Cell Rep.* **42**, 112868 (2023).
82. Silvestri, F. et al. eIF3d specialized translation requires a RACK1-driven eIF3d binding to 43S PIC in proliferating SH-SY5Y neuroblastoma cells. *Cell Signal* **125**, 111494 (2025).
83. Arceo, X. G., Koslover, E. F., Zid, B. M. & Brown, A. I. Mitochondrial mRNA localization is governed by translation kinetics and spatial transport. *PLoS Comput. Biol.* **18**, e1010413 (2022).
84. Lautier, O. et al. Co-translational assembly and localized translation of nucleoporins in nuclear pore complex biogenesis. *Mol. Cell* **81**, 2417–2427 e2415 (2021).
85. Lecuyer, E. et al. Global analysis of mRNA localization reveals a prominent role in organizing cellular architecture and function. *Cell* **131**, 174–187 (2007).
86. Ewels, P. A. et al. The nf-core framework for community-curated bioinformatics pipelines. *Nat. Biotechnol.* **38**, 276–278 (2020).
87. Dobin, A. et al. STAR: ultrafast universal RNA-seq aligner. *Bioinformatics* **29**, 15–21 (2013).
88. Patro, R., Duggal, G., Love, M. I., Irizarry, R. A. & Kingsford, C. Salmon provides fast and bias-aware quantification of transcript expression. *Nat. Methods* **14**, 417–419 (2017).
89. Pelletier, A. R. et al. MealTime-MS: a machine learning-guided real-time mass spectrometry analysis for protein identification and efficient dynamic exclusion. *J. Am. Soc. Mass Spectrom.* **31**, 1459–1472 (2020).

Acknowledgements

The authors acknowledge support from the Canadian Institute for Health Research Project Grant 480523 (D.G.) and National Sciences and Engineering Council Discovery Grant (RGPIN-2019-07234) to D.G. and National Sciences and Engineering Council Discovery Accelerator (RGPAS-2019-00019) to D.G. and a China Council Scholarship (Y.X.). The authors acknowledge technical support from Kristofferson Tandoc. The authors gratefully acknowledge the use and technical support of the following core facilities at the University of Ottawa: Bioinformatics Core Facility (RRID:SCR_022466), Cell Biology and Imaging Core Facility (RRID:SCR_021845), Genome Editing and Molecular Biology Core Facility (RRID:SCR_022954) and the Proteomics Resource Centre.

Author contributions

Y.X. performed the bulk of experiments, helped design experiments, and drafted the manuscript. K.O. performed and analyzed the Western blot. A.S performed FISH staining. K.N. established the APEX2-DFCP1 vectors and cells and contributed to its validation. K.E.K. generated FIP200 knockout cells. R.C.R provided LC3B-mCheery-GFP cell lines and contributed to interpreting results. C.B. contributed to design of experiments and editing. D.G. conceived the project, designed experiments, and wrote the manuscript. All authors reviewed and approved the manuscript.

Competing interests

The authors declare no competing interests.

Additional information

Supplementary information The online version contains supplementary material available at https://doi.org/10.1038/s41467-026-71551-4.

Correspondence and requests for materials should be addressed to Derrick Gibbings.

Peer review information *Nature Communications* thanks Ruijun Tian and the other anonymous reviewer(s) for their contribution to the peer review of this work. A peer review file is available.